

Triiron Complex with *N*-Ferrocenyl Aminocarbyne Ligand Bridging a Diiron Core: DFT, Electrochemical, and Biological Insights

Chiara Saviozzi, Lorenzo Biancalana, Tiziana Funaioli, Marco Bortoluzzi, Michele De Franco, Massimo Guelfi, Valentina Gandin, and Fabio Marchetti*



Cite This: *Inorg. Chem.* 2024, 63, 1054–1067



Read Online

ACCESS |



Metrics & More

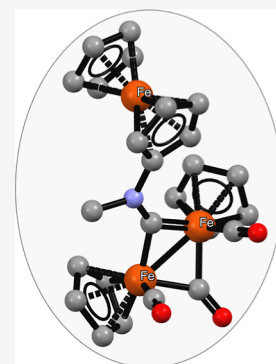


Article Recommendations



Supporting Information

ABSTRACT: The first *N*-ferrocenyl aminocarbyne complex, $[\text{Fe}_2\text{Cp}_2(\text{CO})_2(\mu\text{-CO})\{\mu\text{-CN}(\text{Me})\text{-}(\text{Fc})\}]\text{CF}_3\text{SO}_3$ ($[\mathbf{2}]\text{CF}_3\text{SO}_3$), was synthesized with an 88% yield from $[\text{Fe}_2\text{Cp}_2(\text{CO})_4]$, isocyanoferrrocene (CNFc), and methyl triflate. The synthesis proceeded through the intermediate formation of $[\text{Fe}_2\text{Cp}_2(\text{CO})_3(\text{CNFc})]$, **1**. Multinuclear NMR experiments revealed the presence of *cis* and *trans* isomers for $[\mathbf{2}]\text{CF}_3\text{SO}_3$ in organic solvents, in agreement with DFT outcomes. Electrochemical and spectroelectrochemical studies demonstrated one reduction process occurring prevalently at the diiron core and one oxidation involving the ferrocenyl substituent. The oxidation process is expected to favor the redox activation of $[\mathbf{2}]^+$ in a biological environment. Both $[\mathbf{2}]\text{CF}_3\text{SO}_3$ and its phenyl analogue $[\text{Fe}_2\text{Cp}_2(\text{CO})_2(\mu\text{-CO})\{\mu\text{-CN}(\text{Me})(\text{Ph})\}]\text{CF}_3\text{SO}_3$ ($[\mathbf{3}]\text{CF}_3\text{SO}_3$), prepared for comparison, exerted moderate antiproliferative activity against the human cancer cell lines A431, HCT-15, PSN-1, 2008, and U1285. However, $[\mathbf{2}]\text{CF}_3\text{SO}_3$ exhibited a higher cytotoxicity than $[\mathbf{3}]\text{CF}_3\text{SO}_3$, showed a substantial ability to induce intracellular ROS production, and outperformed cisplatin in a three-dimensional SCLC cell model.



1. INTRODUCTION

The ferrocene skeleton (FeCp_2 , $\text{Cp} = \eta^5\text{-C}_5\text{H}_5$) possesses unique redox behavior, low toxicity, and outstanding stability, and these properties have stimulated research in diverse fields.^{1–3} In particular, the ferrocene scaffold has garnered significant attention for formulating new anticancer metalodrugs.^{4,5} Ferrocenyl compounds typically exert their antiproliferative activity by undergoing Fe^{II} to Fe^{III} oxidation in the tumor environment; this electron transfer disrupts cellular redox homeostasis, ultimately leading to cell death.^{6,7} To harness the beneficial characteristics of ferrocene and create synergistic effects, synthetic chemists have pursued conjugation strategies. Basically, these strategies involve modifying one or two cyclopentadienyl rings of FeCp_2 with suitable functionalities (e.g., phosphine groups, tetradentate Schiff bases, and NHCs) capable of binding to another metal center.^{8,9} Concerning potential medicinal applications, various metal structures with documented biological activities have been attached to ferrocene. Examples include ruthenium(III) complexes analogous to NAMI-A,¹⁰ platinum(II) complexes,^{11,12} and Ru(II)-arene complexes (Figure 1).^{13–15}

Expanding the nuclearity of iron complexes by introducing the ferrocenyl unit can potentially enhance the properties and robustness of the resulting polyiron structures when compared to their lower nuclearity counterparts.^{16,17} In particular, having iron centers in distinct oxidation states may open up multiple redox pathways. For example, attaching a phosphino-ferrocene ligand to a diiron carbonyl core, serving as a model for the active site of $[\text{FeFe}]$ -hydrogenases, was previously found to

optimize the redox catalytic performance of the resulting mixed-valence triiron complex.¹⁸ Interestingly, despite its potential, this approach has been under-explored in the field of medicinal chemistry.

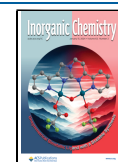
The commercially available compound $[\text{Fe}_2\text{Cp}_2(\text{CO})_4]$ offers an excellent platform for investigating novel reactivity patterns due to its cost-effectiveness and the cooperative effects that arise from the two adjacent metal centers.^{19–21} Two primary classes of derivatives of $[\text{Fe}_2\text{Cp}_2(\text{CO})_4]$, featuring a bridging cationic ligand, can be readily obtained through the sequential assembly of an isocyanide, an alkyl cation, and an alkyne (Figure 1, structures I and II).²² These two families of diiron compounds possess a rare combination of desirable prerequisites for medicinal applications, including a straightforward synthetic procedure, extended structural variability, adequate water solubility enhanced by their ionic nature, and substantial stability in aqueous media.²³ We recently unveiled the promising anticancer potential of selected compounds of types I²⁴ and II.^{25–27} Additionally, we discovered that the incorporation of the ferrocenyl moiety within II using alkynyl ferrocene, $\text{CpFe}(\eta^5\text{-C}_5\text{H}_4\text{C}\equiv\text{CH})$, enhances the antiprolifer-

Received: September 29, 2023

Revised: December 20, 2023

Accepted: December 20, 2023

Published: January 3, 2024



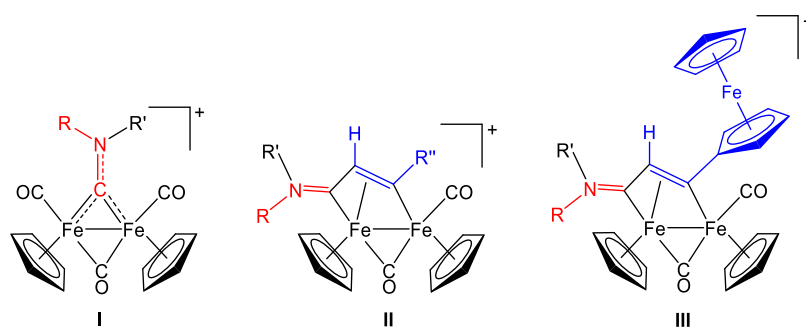
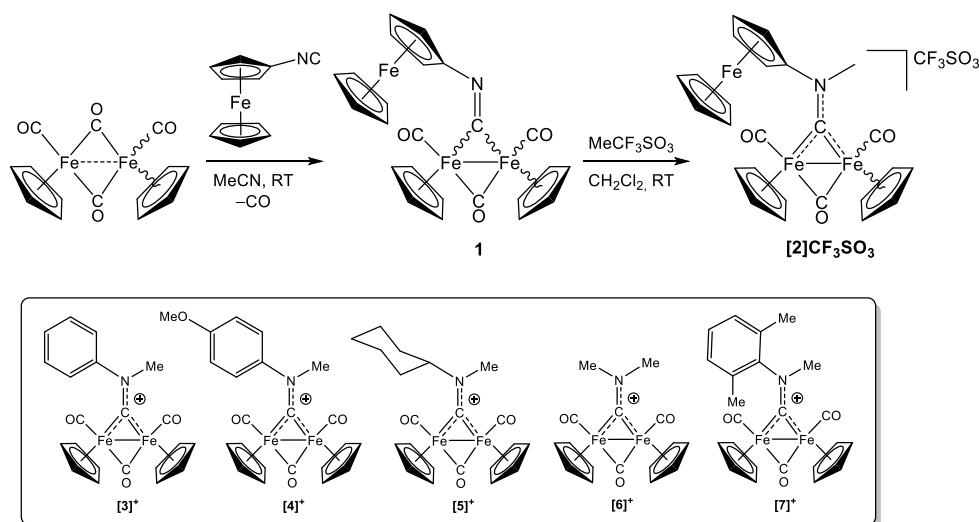


Figure 1. General structures of diiron aminocarbyne complexes (I) derived from $[\text{Fe}_2\text{Cp}_2(\text{CO})_4]$, an isocyanide (CNR, red), and an alkylating agent (R'); their vinyliminium derivatives (II) resulting from the incorporation of an alkyne ($\text{HC}\equiv\text{CR}''$, blue); and including the case of $\text{HC}\equiv\text{CFc}$ (III). CF_3SO_3^- or BF_4^- salts. R , R' = alkyl/aryl groups; R'' = H, alkyl, aryl, pyridyl, thiophenyl, carboxylate, and SiMe_3 .

Scheme 1. Two-step Synthesis of *N*-Ferrocenyl Aminocarbyne Diiron Complex $[2]\text{CF}_3\text{SO}_3$ via Intermediate Formation of an CNFc Adduct (1)^a



^aThe presence of isomeric forms is indicated with wavy bonds; the structures of the isomers of **1** are shown in Figure S3. Inset: related diiron aminocarbyne complexes (triflate salts) employed and/or discussed in this work; **[3]⁺** is reported here for the first time, while **[4]⁺**,²⁴ **[5]⁺**,²⁴ **[6]⁺**,⁴⁷ and **[7]⁺**⁴⁶ were previously described.

ative activity of the resulting complexes (Figure 1, structure III) compared to ferrocenyl lacking analogues.²⁸

Building on this premise, we became interested in incorporating the ferrocenyl unit as a substituent of the compact amino-alkylidene (aminocarbyne²⁹) group in I. It is noteworthy that, while complexes I are normally indefinitely air-stable and robust in a wide range of solvents (including aqueous media), their stability might be sensibly reduced with certain nitrogen substituents (R , R') bearing unfavorable electronic properties (e.g., acetyl/benzoyl groups) or steric bulkiness (*tert*-butyl).^{22,30,31}

Adding a suitable electrophile to a pre-existing isocyanide ligand (M-CNR) represents the most common literature strategy for obtaining aminocarbyne ligands (M-CNRR').^{22,32} Accordingly, the typical synthesis of I involves the initial reaction of $[\text{Fe}_2\text{Cp}_2(\text{CO})_4]$ with an isocyanide, followed by *N*-alkylation.³³

Isocyanoferrrocene (CNFc) is the simplest isocyanide-decorated ferrocene, and its utilization in coordination chemistry has been relatively limited, possibly due to its commercial unavailability and the challenging and tedious synthesis.³⁴ Specifically, examples of CNFc coordination to metal centers has been substantially limited to ruthenium,³⁵

iron phthalocyanine,³⁶ diiron thiolate,³⁷ and chromium complexes, including the unique case of a homoleptic CNFc complex, i.e., $[\text{Cr}(\text{CNFc})_6]$.³⁸ The scarce development of this topic is underscored by the observation that chemical modification of the CNFc ligand has been mostly confined to gold complexes, where amine addition to coordinated CNFc resulted in its conversion into diamino-alkylidene.³⁹

The scarcity of information in this context sharply contrasts with the extensive use of isocyanides as universal and versatile ligands in coordination chemistry.^{40,41}

In this work, we introduce CNFc (for which an optimized synthesis is provided) as a ligand to the $\{\text{Fe}_2\text{Cp}_2(\text{CO})_3\}$ framework and its unprecedented transformation into an aminocarbyne ligand. The overall assembly can be viewed as a triiron system consisting of a Fe^{II} center (ferrocenyl) and a $\text{Fe}^{\text{I}}\text{-Fe}^{\text{I}}$ dinuclear core. We present the structural and electrochemical characterization of the resulting triiron complex, along with a preliminary evaluation of the anticancer potential in both 2D and 3D cell models.

2. RESULTS AND DISCUSSION

2.1. Synthesis, Spectroscopic Characterization, and DFT Analysis.

Initially, CNFc, was synthesized from ferrocene

via the intermediate formation of aminoferrocene using a multistep procedure optimized with respect to the literature (for details, refer to the [Experimental Section](#) and the [Supporting Information](#)). Subsequently, the reaction between $[\text{Fe}_2\text{Cp}_2(\text{CO})_4]$ and freshly prepared CNFc, in a 1:1 molar ratio, was conducted in acetonitrile at room temperature and proceeded with the selective substitution of one carbonyl ligand with CNFc ([Scheme 1](#)). This aspect is nontrivial, as it is documented that allowing $[\text{Fe}_2\text{Cp}_2(\text{CO})_4]$ to react with one equivalent of isocyanides can lead to multiple CO–CNR substitutions, resulting in mixtures of products.³²

Based on infrared spectroscopy measurements, $[\text{Fe}_2\text{Cp}_2(\text{CO})_3(\text{CNFc})]$, **1** – an uncommon example of an CNFc coordination complex (see [Introduction](#)) – is believed to exist in solution as a mixture of four interconverting isomers. These isomers vary in the relative orientation of the Cp ligands (cis or trans) and the coordination site of the CNFc ligand (terminal or bridging), see [Figure S3](#). This situation aligns with the general case of $[\text{Fe}_2\text{Cp}_2(\text{CO})_3(\text{CNR})]$ complexes (R = alkyl or aryl).^{32,42,43} Exception arising when bulkier R groups (e.g., 2,6-dimethylphenyl and cyclohexyl) are present, disfavoring the bridging CNR coordination.³² The interconversion of isomers in solution was previously elucidated to follow the Adams–Cotton mechanism, which entails the formation of bridge-opened intermediates (comprising only terminal ligands bound to the diiron core), where rotation around the Fe–Fe bond is permitted.^{32,44}

In the case of **1**, cis and trans isomers display the IR bands accounting for the terminal CO ligands at 1988 and 1951 cm^{-1} , respectively (CH_2Cl_2 solution). Prior research has demonstrated that the isomeric composition of $[\text{Fe}_2\text{Cp}_2(\text{CO})_3(\text{CNR})]$ complexes is usually solvent-dependent, with polar solvents favoring the more polar cis isomer over the trans isomer.⁴⁵ In agreement with this observation, both cis-**1** and trans-**1** were detected in comparable amounts in CH_2Cl_2 ($\mu = 1.60$ D) solution, while cis-**1** was prevalent in MeCN ($\mu = 3.92$ D), [Figure S4](#).

The coordination mode of the CNFc ligand in **1** can be deduced from the corresponding CN stretching vibration, appearing at 2100 and 1691 cm^{-1} for terminal ($\text{C}\equiv\text{N}$) and bridging ($\text{C}=\text{N}$) coordination, respectively.^{32,46} A comparative analysis of IR spectra suggests that the bridging-isocyanide isomers are slightly favored in acetonitrile solution compared to dichloromethane ([Figures S3 and S4](#)). The wavenumber associated with the terminal CNFc is lower than that of noncoordinated CNFc (2122 cm^{-1} in CH_2Cl_2 solution), indicating a significant occurrence of Fe \rightarrow CNFc π -backdonation in **1**.^{32,41}

The crude solid residue obtained from $[\text{Fe}_2\text{Cp}_2(\text{CO})_4]$ and CNFc was dissolved in dichloromethane and treated with methyl triflate, yielding the *N*-ferrocenyl aminocarbyne complex $[\mathbf{2}]\text{CF}_3\text{SO}_3$. Notably, $[\mathbf{2}]\text{CF}_3\text{SO}_3$ could be purified through alumina chromatography without decomposition³⁰ and was isolated as an air-stable red solid in 88% yield ([Scheme 1](#)).

The ^1H NMR spectrum of $[\mathbf{2}]\text{CF}_3\text{SO}_3$ in CDCl_3 revealed the presence of two sets of signals in an approximately 5:1 ratio, which were assigned to cis and trans isomers, respectively, based on NOESY evidence ([Figures S6, S7, and S9](#)). It is noteworthy that cis–trans isomerism has been rarely observed in diiron compounds of the type $[\text{Fe}_2\text{Cp}_2(\text{CO})_2(\mu\text{-CO})\{\mu\text{-CN}(\text{R})(\text{R}')\}]^+$, and specifically only for R = R' = Me or Et.⁴⁸

DFT calculations conducted on $[\mathbf{2}]^+$ (PBEh-3c method, CHCl_3 as a continuous medium) pointed out that the cis isomer is more stable than the trans one by 1.4 kcal/mol. This energy difference corresponds to a predicted cis/trans ratio of ≈ 11 , at 298 K. The DFT-optimized geometries of cis- $[\mathbf{2}]^+$ and trans- $[\mathbf{2}]^+$ are shown in [Figure 2](#), and the most salient calculated bonding parameters are provided in the caption.

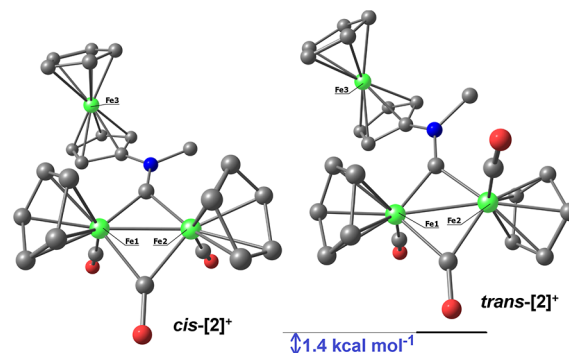
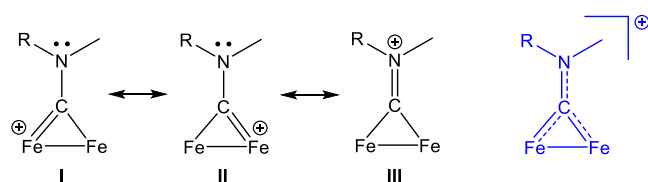


Figure 2. DFT-optimized geometries of cis- $[\mathbf{2}]^+$ (left) and trans- $[\mathbf{2}]^+$ (right), computed at PBEh-3c level (CHCl_3 as a continuous medium). Fe, green; N, blue; and C, gray. Hydrogen atoms were omitted for clarity. Selected computed bond lengths for cis- $[\mathbf{2}]^+$ (Å): Fe1–C(carbyne) 1.856; Fe2–C(carbyne) 1.894; carbyne–N 1.297; Fe1–Fe2 2.482; Fe1–C(CO) 1.776; Fe2–C(CO) 1.774; Fe1–C(μ -CO) 1.935; Fe2–C(μ -CO) 1.893; average Fe1–C(Cp) 2.112; average Fe2–C(Cp) 2.115; and average Fe3–C(Cp) 2.058. Selected computed bond lengths for trans- $[\mathbf{2}]^+$ (Å): Fe1–C(carbyne) 1.841; Fe2–C(carbyne) 1.875; carbyne–N 1.298; Fe1–Fe2 2.505; Fe1–C(CO) 1.780; Fe2–C(CO) 1.780; Fe1–C(μ -CO) 1.933; Fe2–C(μ -CO) 1.905; average Fe1–C(Cp) 2.119; average Fe2–C(Cp) 2.116; and average Fe3–C(Cp) 2.056.

The geometric parameters extracted from the calculated DFT structures are in line with those observed in other diiron aminocarbyne complexes, as reported previously.^{24,46} In particular, the carbyne–nitrogen bond distance (1.297 Å in the cis isomer) is indicative of a partial iminium character. Besides, the average Fe–carbyne distance (1.875 Å in the cis isomer) is considerably shorter than the average Fe– μ -CO distance (1.914 Å in the cis isomer). These data highlight the greater π -acceptor ability of the (ferrocenyl)aminocarbyne ligand compared to the CO ligand.^{22,49} This leads the aminocarbyne to preferentially occupy a bridging coordination site over a terminal one, as such an arrangement enhances the electron backdonation from the iron atoms.²² The bonding situation in $[\mathbf{2}]^+$ can be therefore described in terms of the resonance forms depicted in [Scheme 2](#). In detail, the competition for the vacant p-orbital on the carbyne carbon, between the nitrogen lone pair and the backdonation from the irons results in a substantial charge delocalization.

The experimentally detected cis/trans ratio (=5 in CDCl_3 solution) is significantly lower than the theoretical value (11, in CHCl_3 as a continuous medium). In general, the cis/trans isomerization for cationic tris-carbonyl μ -aminocarbyne complexes is not accessible at least up to 50 °C.^{47,50} Therefore, to promote a potential isomerization process, solutions of $[\mathbf{2}]\text{CF}_3\text{SO}_3$ in various solvents were heated ([Table 5](#)). The greatest change in the cis/trans ratio was achieved by refluxing an acetone solution of $[\mathbf{2}]\text{CF}_3\text{SO}_3$ for 2.5 h, resulting in an 18:1 cis/trans ratio. Consistently, DFT calculations considering acetone as an implicit solvent pointed out that cis- $[\mathbf{2}]^+$ is

Scheme 2. Bonding of the Bridging {CN(Me)R} Ligand (Including R = Fc as in [2]⁺) to the {Fe₂Cp₂(CO)₃} Fragment: I, II: Aminocarbyne Resonance Structures; III: Iminium Resonance Structure^a



^aIn blue, comprehensive representation with a delocalized positive charge.

Table 1. Formal Electrode Potentials (V, vs FeCp₂ and, in Brackets, vs Ag/AgCl) and Peak-To-Peak Separations (mV) for the Redox Processes Exhibited in CH₂Cl₂ or THF Solutions and Aqueous Media by [2]⁺, [3]⁺, [4]⁺, and [5]⁺

compound	oxidation processes			reduction process		
	E_1°	$\Delta E_p^{a,c}$	E_2°	$\Delta E_p^{a,c}$	E_3°	
[2] CF ₃ SO ₃ ^b	+1.28 ^e (+1.73)		+0.28 (+0.73)	80	-1.44 (-0.99)	83
[3] CF ₃ SO ₃ ^b	+0.97 (+1.42)	101			-1.41 (-0.96)	88
[4] CF ₃ SO ₃ ^b	+0.97 (+1.42)	95			-1.40 (-0.95)	84
[5] CF ₃ SO ₃ ^b	+0.95 (+1.40)	120			-1.41 (-0.96)	84
[2] CF ₃ SO ₃ ^c	+0.24 (+0.81)	85			-1.42 (-0.85)	85
[3] CF ₃ SO ₃ ^c	+1.03 ^e (+1.60)				-1.40 (-0.83)	80
[4] CF ₃ SO ₃ ^c	+1.05 ^e (+1.62)				-1.42 (-0.85)	80
[4] CF ₃ SO ₃ ^d	+0.90 ^e (+1.10)				-1.17 (-0.97)	96
[5] CF ₃ SO ₃ ^d	+0.90 ^e (+1.10)				-1.18 (-0.98)	96

^aMeasured at 0.1 V/s. ^bIn CH₂Cl₂/[ⁿBu₄N]PF₆. ^cIn THF/[ⁿBu₄N]-PF₆. ^dIn phosphate buffer. ^ePeak potential value for irreversible processes.

Table 2. Behavior of Diiron Aminocarbyne Complexes in Aqueous Solutions (See Experimental Section for Details)^a

	[2]CF ₃ SO ₃	[3]CF ₃ SO ₃
solubility/mol·L ⁻¹	<3 × 10 ^{-4b}	1.6 × 10 ⁻³
Log <i>P</i> _{ow}	0.55 ± 0.05	-0.38 ± 0.02
residual complex % in D ₂ O/CD ₃ OD	62%	68%
residual complex % in DMEM-d/CD ₃ OD	65%	74%

^aSolubility in D₂O (¹H NMR, Me₂SO₂ internal standard) and octanol/water partition coefficient (Log *P*_{ow}; UV-vis) at 21 ± 1 °C. Relative stability in D₂O/CD₃OD and DMEM-d/CD₃OD mixtures (5:2 v/v) at 37 °C after 48 or 24 h, respectively (¹H NMR, Me₂SO₂ internal standard). ^bBelow the lowest value of quantitation.

more stable than trans-[2]⁺ by approximately 1.7 kcal mol⁻¹, corresponding to a cis/trans ratio of 17 at 298 K. However, some degradation was observed in all tested conditions, leading to the formation of non carbonyl byproducts that could not be identified. We presume that the isomerization process, if any, follows the Adams–Cotton mechanism via a terminal aminocarbyne species (see above).²² In the NMR spectra of [2]CF₃SO₃ (Figures S6–S8), each isomer displays non-equivalent Cp ligands within the {Fe₂Cp₂(CO)₃} core due to

the double bond character of the μ-C–N bond (vide infra), which hinders rotation around the C–N axis [e.g., for cis-[2]⁺: δ(¹H) = 5.36, 4.84 ppm; δ(¹³C) = 90.5, 90.4 ppm]. The Cp ring belonging to the ferrocenyl moiety exhibits lower chemical shift values [δ = 4.43 (¹H) and 70.5 ppm (¹³C) for cis-[2]⁺]. The predominant cis isomer displays ¹³C NMR resonances for the carbonyl ligands at 255.3 (bridging CO) and 209.1 and 207.9 ppm (terminal CO). Accordingly, the IR spectrum of [2]CF₃SO₃ (in CH₂Cl₂) contains three bands associated with the stretching vibrations of the terminal (2024 and 1992 cm⁻¹) and bridging carbonyl ligands (1837 cm⁻¹). Notably, the IR absorptions for the two isomers are almost identical, with the bands substantially overlapping (Figure S5).

Key spectroscopic features are those related to the {μ-CN} unit, manifesting in an infrared absorption at 1527 cm⁻¹ and a ¹³C NMR resonance at 326.8 ppm. Literature data concerning diiron aminocarbyne complexes of general formula [Fe₂Cp₂(CO)₂(μ-CO){μ-CN(Me)(R)}]⁺ range from 1522 (R = 2,6-C₆H₃MeCl) to 1604 cm⁻¹ (R = Me) and 331.5 (R = 2,6-C₆H₃MeCl) to 315.5 ppm (R = Me), respectively, and clearly correlate with the electron donor properties of the R substituent.^{22,24} The values obtained for [2]CF₃SO₃ (R = Fc) approximate those of the analogous complex with R = 2,6-C₆H₃MeCl, outlining that the ferrocenyl moiety behaves electronically as an aryl within the cationic aminocarbyne moiety. We note that ferrocenyl has been previously regarded as an electron donor group in various systems; for instance, its donor capability has been estimated to exceed that of the methyl group in organophosphorus compounds,⁵¹ and to approximate that of the 4-aminophenyl within W propargylidene complexes.⁵²

For sake of comparison, we synthesized the unprecedented *N*-phenyl aminocarbyne complex [Fe₂Cp₂(CO)₂(μ-CO){μ-CN(Me)(Ph)}]CF₃SO₃, [3]CF₃SO₃, following the two-step method described for [2]CF₃SO₃ (Scheme 1). Briefly, freshly prepared phenyl isocyanide (from phenyl formamide, see the Experimental Section) was allowed to react with [Fe₂Cp₂(CO)₄] in acetonitrile at room temperature. This reaction resulted in the formation of the known dark-violet compound [Fe₂Cp₂(CO)₂(μ-CO)(μ-CNPh)],^{53–56} which was isolated through alumina chromatography. Subsequent methylation with CF₃SO₃Me in CH₂Cl₂ followed by chromatographic purification, afforded a red powder of the aminocarbyne complex [3]CF₃SO₃. The latter was isolated in ca. 41% yield, together with a minor amount of [Fe₂Cp₂(CO)-(CNPh)(μ-CO){μ-CN(Me)(Ph)}]⁺ (unprecedented). The moderate yield and the formation of byproducts appear ascribable to the thermal instability and the enhanced reactivity of phenyl isocyanide promoted by metal coordination. The thermal or photolytic displacement of CO from [Fe₂Cp₂(CO)₄] using PhNC was previously found to give [Fe₂Cp₂(CO)₂(μ-CO)(μ-CNPh)] in 10–50% yields, in admixture with the disubstituted derivative [Fe₂Cp₂(CO)₂(CNPh)₂].^{51,52} A similar reaction involving [Ru₂Cp₂(CO)₄] resulted in the complete decomposition of the isocyanide.⁴⁴ Additionally, [Fe₂Cp₂(CO)₂(μ-CO)(μ-CNPh)] was obtained in low to modest yields (5–46%) from other monoiron or diiron precursors.^{53,54}

The novel *N*-phenyl aminocarbyne complex [3]CF₃SO₃ is air-stable and was characterized by IR and NMR spectroscopy (Figures S10–S14). The spectroscopic data for the {μ-CN} moiety well match the corresponding ones for [2]CF₃SO₃ (IR absorption at 1527 and 1531 cm⁻¹ and ¹³C NMR resonance at

326.8 and 324.5 ppm, respectively, in $[2]CF_3SO_3$ and $[3]CF_3SO_3$).

The cation $[3]^+$ was computationally optimized at the C-PCM/PBEh-3c level, considering $CHCl_3$ as the solvent. Interestingly, the cis isomer exhibited higher stability than the trans isomer by about 3.7 kcal mol⁻¹. This outcome aligns with the experimental detection of a single species, cis- $[3]^+$, in solution. The DFT-optimized structure of cis- $[3]^+$ is shown in Figure 3 and selected computed bond lengths are collected in the caption. Figure S15 shows a comparative view of the cis and trans isomers of $[3]^+$.

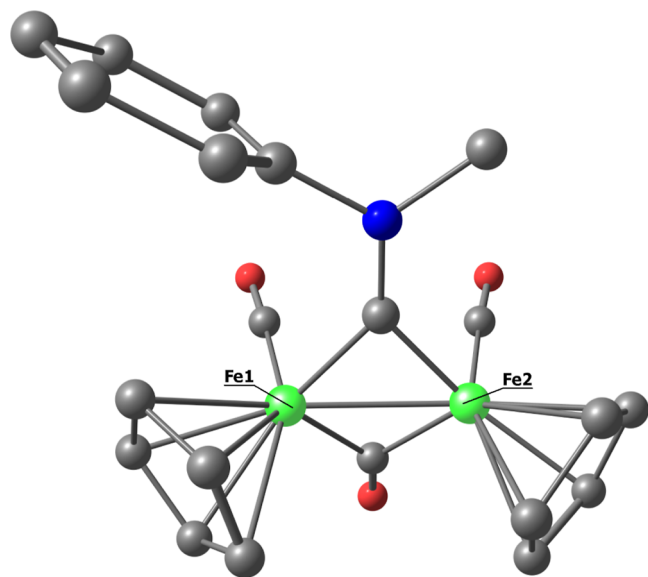


Figure 3. DFT optimized geometry of cis- $[3]^+$, computed at PBEh-3c level ($CHCl_3$ as a continuous medium). Fe, green; N, blue; and C, gray. Hydrogen atoms were omitted for clarity. Selected computed bond lengths: Fe1–C(carbyne) 1.859; Fe2–C(carbyne) 1.844; C(carbyne)–N 1.291; Fe1–Fe2 2.491; Fe1–C(CO) 1.774; Fe2–C(CO) 1.772; Fe1–C(μ -CO) 1.903; Fe2–C(μ -CO) 1.937; average Fe1–C(Cp) 2.105; and average Fe2–C(Cp) 2.107.

In order to compare the electronic properties of the ferrocenyl- and phenyl-substituted aminocarbyne ligands, extended charge decomposition analyses (ECDA)⁵⁷ were carried out. A positive charge was assigned to the aminocarbyne moiety. The net electron transfer from $\{Fe_2Cp_2(CO)_2(\mu-CO)\}$ to $[CN(Me)Fc]^+$ is calculated to be 0.754, and a closely related value of 0.784 was determined for $[CN(Me)Ph]^+$. This similarity of values suggests that, overall, the two ligands exhibit comparable coordination features and electronic trends, in agreement with the key spectroscopic data discussed above. Furthermore, it is remarkable that the carbonyl regions of the simulated IR spectra of $[2]^+$ and $[3]^+$ are superimposable, as evident in Figure S16.

2.2. Electrochemical Studies and DFT Results. The redox chemistry and the in situ IR spectroelectrochemistry (IR SEC) of $[2]CF_3SO_3$ and $[3]CF_3SO_3$ were investigated in dichloromethane and THF solutions containing $[nBu_4N]PF_6$ (0.2 mol dm⁻³) as the supporting electrolyte. The aminocarbyne complexes $[4]CF_3SO_3$ and $[5]CF_3SO_3$ (Scheme 1) were included in this study for comparative purposes. Table 1 collects the formal electrode potentials of the observed redox changes.

The presence of the ferrocenyl substituent within $[2]^+$ becomes evident from the comparison of the cyclic voltammograms of $[2]^+$ and $[3]^+$ in the positive potential region. In CH_2Cl_2 solution, $[2]^+$ displays one diffusion controlled, mono-electronic oxidation at +0.28 V vs $FeCp_2$. This process exhibits features of chemical reversibility in the cyclic voltammetric time scale (Figure 4a) and can be

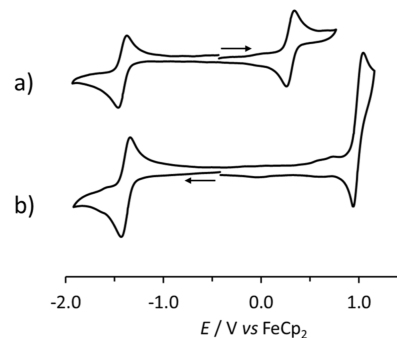


Figure 4. CV recorded at a Pt electrode in a CH_2Cl_2 solution of (a) $[2]^+$ between -1.92 and $+0.72$ V; (b) $[3]^+$ between -1.92 and $+1.16$ V. $[nBu_4N]PF_6$ (0.2 mol dm⁻³) as a supporting electrolyte. Scan rate: 0.1 V s⁻¹. Arrows indicate the direction of the scan.

attributed to the Fe^{II} -ferrocenyl moiety of the triiron complex. On the other hand, a two-electron, partially chemically reversible oxidation at a higher potential (about +0.97 V vs $FeCp_2$) was observed in the CV profiles of $[3]^+$ (Figure 4b), $[4]^+$, and $[5]^+$ (Table 1). This result seems consistent with a previous electrochemical study conducted on $[6]CF_3SO_3$ and $[7]CF_3SO_3$ in acetonitrile.⁵⁸

When the oxidation process of $[2]^+$ was investigated by in situ IR-SEC in an optically transparent thin-layer electrochemical (OTTLE) cell,⁵⁹ a blueshift of the IR absorption bands due to CO-stretching modes of terminal and bridging CO ligands of $[2]^+$ (from 2024, 1992, and 1837 cm⁻¹ to 2033, 2002, and 1845 cm⁻¹) was detected as the working electrode (WE) potential increased from +0.1 to +0.5 V (vs $FeCp_2$), Figure 5. This shift corresponds to the quantitative formation of the one-electron oxidation product $[2]^{2+}$. The latter remained stable within the time scale of the spectroelec-

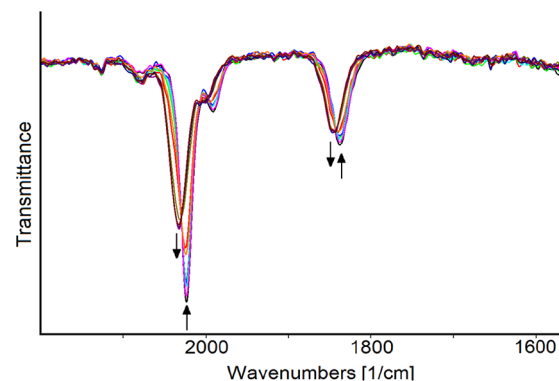


Figure 5. IR spectra of a CH_2Cl_2 solution of $[2]CF_3SO_3$ recorded in an OTTLE cell during the progressive increase of the WE potential from +0.1 to +0.5 V (vs $FeCp_2$; scan rate 1 mV sec⁻¹). $[nBu_4N]PF_6$ (0.2 mol dm⁻³) as the supporting electrolyte. Absorptions of the solvent and supporting electrolyte have been subtracted.

trochemical experiment; indeed, the initial spectrum was almost completely restored during the reverse reduction scan.

The slight shift (approximately $+10\text{ cm}^{-1}$) of the wavenumbers agrees with the assumption that the reversible one-electron removal primarily affects the ferrocenyl portion of the complex, thereby having minimal impact on the carbonyl ligands bound to the Fe_2Cp_2 core.

In the negative potential range, all the complexes $[2]^+ - [5]^+$ undergo a mono-electronic, diffusion controlled, and electrochemically reversible reduction at approximately the same potential. However, this reduction is complicated by subsequent chemical reactions (with i_b/i_f ratios of 0.84 and 0.83 at a scan rate of 100 mV s^{-1} for $[2]^+$ and $[3]^+$, respectively).

Collectively, the in situ IR SEC analyses of $[2]^+ - [5]^+$ in $\text{CH}_2\text{Cl}_2/[\text{nBu}_4\text{N}]\text{PF}_6$ solutions indicate that electron addition mainly involves the $[\text{Fe}^{\text{I}}\text{Fe}^{\text{I}}]$ core.

As the potential of the working electrode gradually decreased from -1.3 to -1.6 V (vs FeCp_2), the IR absorptions of $[2]^+$ were initially replaced by new bands at lower wavenumbers ($\nu_{\text{CO}} = 1958, 1919,$ and 1741 cm^{-1} , Figure S17a), attributed to the neutral radical species $[2]^\bullet$. However, prior to the complete disappearance of $[2]^+$, a slight blueshift of the IR absorption bands due to the stretching modes of terminal and bridging CO ligands of the newly formed $[2]^\bullet$ was detected ($\nu_{\text{CO}} = 1963, 1928,$ and 1773 cm^{-1} , Figure S17b). This process was completed within the following 10 min during microelectrolysis at a constant potential of -1.8 V (Figure S17c). Instead, the spectral changes recorded in the OTTLE cell over 10 min after the complete reduction of $[2]^+$, without an applied potential, suggest that a disproportionation reaction of $[2]^\bullet$ occurs subsequent to the electron transfer. This reaction results in the regeneration of $[2]^+$ and the formation of an unidentified species, 2^* ($\nu_{\text{CO}} = 1963, 1928,$ and 1773 cm^{-1} , Figure S18). Evidence of a disproportionation reaction of $[2]^\bullet$ and the bulk electrolysis to determine the electron stoichiometry of the transformation $[2]^+ \rightarrow 2^*$ (Figure S19) is supplied in the Supporting Information.

The formation of the tris-carbonyl complex 2^* ($\nu_{\text{CO}} = 1963, 1928,$ and 1773 cm^{-1}) is restricted to the use of dichloromethane as solvent, and we hypothesize that it is consequent to the generation of radical species (X) from CH_2Cl_2 , converting the bridging aminocarbyne ligand, $\text{CN}(\text{Me})(\text{Fc})$, into a bridging aminocarbene, $\text{C}(\text{X})\text{N}(\text{Me})(\text{Fc})$.⁴⁶ We verified that in $\text{THF}/[\text{nBu}_4\text{N}]\text{PF}_6$ solutions, the reduction of $[2]^+$ is fully reversible ($i_b/i_f = 1$ at a scan rate of 100 mV s^{-1}) (Table 1) and, consistently, an IR SEC experiment confirmed that the reduction of $[2]^+$ ($\nu_{\text{CO}} = 2016, 1986,$ and 1834 cm^{-1}) leads to the quantitative and entirely reversible formation of $[2]^\bullet$ ($\nu_{\text{CO}} = 1956, 1919,$ and 1757 cm^{-1}), also in the long time scale of this experiment (Figure 6).

A parallel behavior was observed for $[3]^+ - [5]^+$, in both CH_2Cl_2 and THF (Figure S20 refers to $[3]^+$ as a representative compound), confirming that the reactivity of the radicals $[2]^\bullet - [5]^\bullet$ in dichloromethane is a general trend, which is related to the intervention of the solvent and independent of the presence of the ferrocenyl moiety.⁶⁰ The large redshift of the IR absorption bands due to stretching modes of terminal and bridging CO ligands upon reduction (about 70 cm^{-1} for both complexes) suggests that the LUMO is mainly localized on the Cp_2Fe_2 core, in agreement with previous DFT outcomes on the *N*-dimethyl derivative $[6]^+$ (Scheme 1).⁶¹

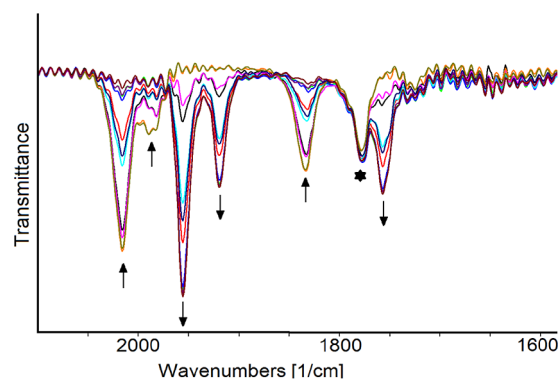


Figure 6. IR spectra of a THF solution of $[2]^+$ recorded in an OTTLE cell during the progressive decrease of the WE potential from -1.2 to -1.6 V (vs FeCp_2 ; scan rate 1 mV s^{-1}) starred peak is due to impurities. $[\text{nBu}_4\text{N}]\text{PF}_6$ (0.2 mol dm^{-3}) as the supporting electrolyte. Absorptions of the solvent and supporting electrolyte have been subtracted.

The structures of both the cis and trans isomers of the radical $[2]^\bullet$ were computationally optimized and are shown in Figure 7. The cis- $[2]^\bullet$ isomer resulted more stable than trans-

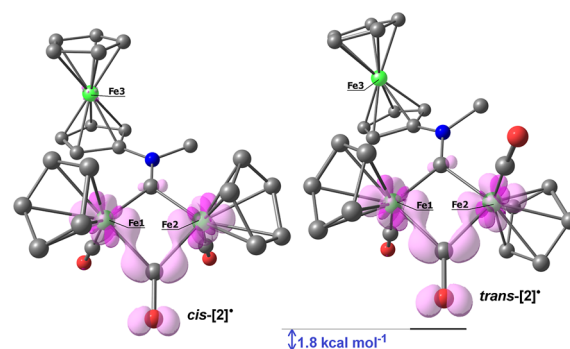


Figure 7. DFT-optimized geometries of cis- $[2]^\bullet$ (left) and trans- $[2]^\bullet$ (right), computed at PBEh-3c level (acetone as a continuous medium). Fe, green; N, blue; and C, gray. Hydrogen atoms were omitted for clarity. Spin density surfaces (isovalue = 0.01 au) in pink tones. Selected computed bond lengths for cis- $[2]^\bullet$ (\AA): Fe1–C(carbyne) 1.886; Fe2–C(carbyne) 1.917; C–N 1.310; Fe1–Fe2 2.678; Fe1–C(CO) 1.743; Fe2–C(CO) 1.745; Fe1–C(μ -CO) 1.931; Fe2–C(μ -CO) 1.916; average Fe1–C(Cp) 2.176; average Fe2–C(Cp) 2.158; and average Fe3–C(Cp) 2.058. Selected computed bond lengths for trans- $[2]^\bullet$ (\AA): Fe1–C(carbyne) 1.873; Fe2–C(carbyne) 1.899; C–N 1.311; Fe1–Fe2 2.714; Fe1–C(CO) 1.748; Fe2–C(CO) 1.752; Fe1–C(μ -CO) 1.930; Fe2–C(μ -CO) 1.930; average Fe1–C(Cp) 2.178; average Fe2–C(Cp) 2.158; and average Fe3–C(Cp) 2.057.

$[2]^\bullet$ by approximately 1.8 kcal mol^{-1} , considering acetone as the continuous medium. The optimized structures closely resemble those of the parent cations, exhibiting root-mean-square deviation (RMSD) values ranging from 0.118 to 0.133 \AA . This outcome is in line with the electrochemical reversibility described above. The simulated IR spectra of cis- $[2]^\bullet$ and trans- $[2]^\bullet$, compared to the corresponding parent cationic complexes, highlight the significant shift of the carbonyl stretching vibrations toward lower wavenumbers (Figure S22). The spin density plots depicted in Figure 7 confirm that the reduction process involves the $\{\text{Fe}(\mu\text{-CO})\text{Fe}\}$ fragment, while the contribution of the ferrocenyl unit appears negligible.

Table 3. Cytotoxic Activity of Diiron Complexes and Cisplatin in 2D Models

IC ₅₀ (μM) ± SD.	A431	HCT-15	PSN-1	2008	U1285
[2]CF ₃ SO ₃	60 ± 14	33 ± 12	23.1 ± 4.6	32.9 ± 2.8	16.0 ± 1.3
[3]CF ₃ SO ₃	75.1 ± 8.9	86.2 ± 0.5	>100	86 ± 11	50.8 ± 6.7
cisplatin	1.7 ± 0.3	13.9 ± 1.6	12.1 ± 2.8	2.1 ± 1.1	6.9 ± 1.1

In summary, within the triiron species [2]⁺, the two iron-based redox systems (i.e., the ferrocenyl Fe^{II} and Fe^IFe^I) are independent.

The redox properties of [4]CF₃SO₃ and [5]CF₃SO₃ were additionally investigated in a phosphate buffer (PB; pH = 7.3), given the sufficient solubility of these complexes in aqueous media. In the PB, the oxidation process for both [4]⁺ (Figure S21) and [5]⁺ is irreversible, multielectronic, and shifted at lower potentials by approximately 300 mV compared to the organic solvent.⁶² Conversely, a reduction occurs at potential values similar to those recognized in CH₂Cl₂ solution. In the backscan, we observed an absorption peak, probably due to the neutral complexes 4[•] and 5[•].

Anyway, both the reduction and oxidation potentials of [4]⁺ and [5]⁺ fall outside the biologically relevant potential range, which approximately covers the window −0.4 to +0.8 V vs SHE (−0.6 to +0.6 V vs Ag/AgCl).^{63,64} The limited water solubility of [2]CF₃SO₃ prevented its CV characterization in the PB solution. Nevertheless, if we assume that the behavior difference of [2]⁺ when varying the solvent parallels that of [4]⁺ and [5]⁺, the potential for achieving biooxidative activation could be accessible for the *N*-ferrocenyl aminocarbyne complex.

2.3. Behavior of Diiron Complexes in Aqueous Media and Biological Studies. In preparation for the biological investigation, we conducted an initial assessment of [2]-CF₃SO₃ and [3]CF₃SO₃ in aqueous solutions. By using established ¹H NMR and UV–vis methods, we assessed the water (D₂O) solubility, the octanol–water partition coefficient, and the stability of the complexes under conditions relevant to biology (37 °C, cell culture medium), see Table 2. The change from a phenyl to a ferrocenyl group in the aminocarbyne ligand is accompanied by decreased water solubility and increased lipophilicity. Nevertheless, both [2]CF₃SO₃ and [3]CF₃SO₃ can be categorized as *amphiphilic* compounds (−0.5 < Log *P*_{ow} < +0.5). These compounds exhibited substantial stability at 37 °C, with 62–74% of the starting material remaining unchanged after 48 h in D₂O solution or after 24 h in DMEM cell culture medium.⁶⁵

Interestingly, ¹H NMR spectroscopy showed for the aqueous solutions of [2]⁺ an enrichment in the *trans* isomer (*cis/trans* ratio ≈ 1), deviating from the situation observed in CDCl₃ (see above). We did not collect evidence of an oxidation of the ferrocenyl unit in [2]⁺ in such aerobic environments (*E*^o = +0.83 V vs SHE for O₂/H₂O at pH = 7).

Several diiron aminocarbyne complexes were previously investigated for their *in vitro* anticancer activity (see Introduction), which is strongly influenced by the nature of the aminocarbyne substituents (Figure 1, structure I). For instance, while [6]CF₃SO₃ does not exhibit cytotoxicity, [4]CF₃SO₃ and [5]CF₃SO₃ have showcased a significant antiproliferative activity against various human cancer cell lines.^{23,24} Their mechanism of action has been mainly associated with their capacity to interfere with cellular redox processes through the intracellular release of iron(I) species.²⁴ The incorporation of the ferrocenyl in [2]CF₃SO₃ introduces

an additional redox-active fragment that could potentially participate in intracellular biological processes (see Introduction). On the other hand, [3]CF₃SO₃, lacking the ferrocenyl unit, serves as a benchmark for comparison,⁶⁶ especially when considering the similar electronic properties revealed by the bridging ligands CNMe(Fc) (in [2]⁺) and CNMe(Ph) (in [3]⁺), *vide infra*.

The cytotoxicity of [2]CF₃SO₃ and [3]CF₃SO₃ was evaluated across a range of human cancer cell lines representative of different solid tumors. In particular, the in-house cancer cell panel includes examples of human cervical (A431), colon (HCT-15), pancreatic (PSN-1), and ovarian (2008) carcinoma, as well as small-cell lung cancer (SCLC, U1285). The cytotoxicity parameters, expressed in terms of IC₅₀ values acquired following 72 h of exposure to the MTT assay, are reported in Table 3. For comparison purposes, the cytotoxicity of the reference metal-based chemotherapeutic drug cisplatin was assessed under the same experimental conditions.

Cells [(3–8) × 10³ cell/well] were treated for 72 h with increasing concentrations of tested compounds. Cytotoxicity was assessed by MTT test. The IC₅₀ values were calculated by the four-parameter logistic model (*p* < 0.05). SD is the standard deviation.

Both [2]CF₃SO₃ and [3]CF₃SO₃ showed a moderate cytotoxicity profile, with average IC₅₀ values generally higher compared to cisplatin over the five tested human cancer cell lines. Within the diiron complexes, the ferrocenyl derivative [2]CF₃SO₃ is significantly more effective than the *N*-phenyl analogue [3]CF₃SO₃. On average, the *in vitro* antitumor activity of [2]CF₃SO₃ exceeded that of [3]CF₃SO₃ by a factor of 2.4. In particular, [2]CF₃SO₃ outperformed [3]CF₃SO₃ against pancreatic adenocarcinoma (PSN-1) and SCLC cells, showing 4-fold and 3-fold higher efficacy, respectively.

Although 2D cell cultures are widely employed for *in vitro* screening due to their low cost, simplicity, and reliability, they are unable to mimic the properties of *in vivo* solid tumors. In contrast, 3D cell cultures offer greater efficiency in reproducing the heterogeneity and complexity of tumor masses, and therefore they are more predictive of *in vivo* outcomes than traditional 2D cell cultures.⁶⁷ On these bases, the cytotoxicity of [2]CF₃SO₃ and [3]CF₃SO₃ was also examined using a 3D cell culture model of SCLC cells. Hence, U1285 cells were treated with the investigated compounds for 72 h, and cell viability was assessed by means of the acid phosphatase (APH) assay (Table 4).

Spheroids (2.5 × 10³ cells/well) were treated for 72 h with increasing concentrations of tested compounds. The growth-

Table 4. Cytotoxic Activity of Diiron Complexes and Cisplatin in a SCLC 3D Model

IC ₅₀ (μM) ± SD.	U1285
[2]CF ₃ SO ₃	51.3 ± 4.2
[3]CF ₃ SO ₃	>100
cisplatin	65.4 ± 1.4

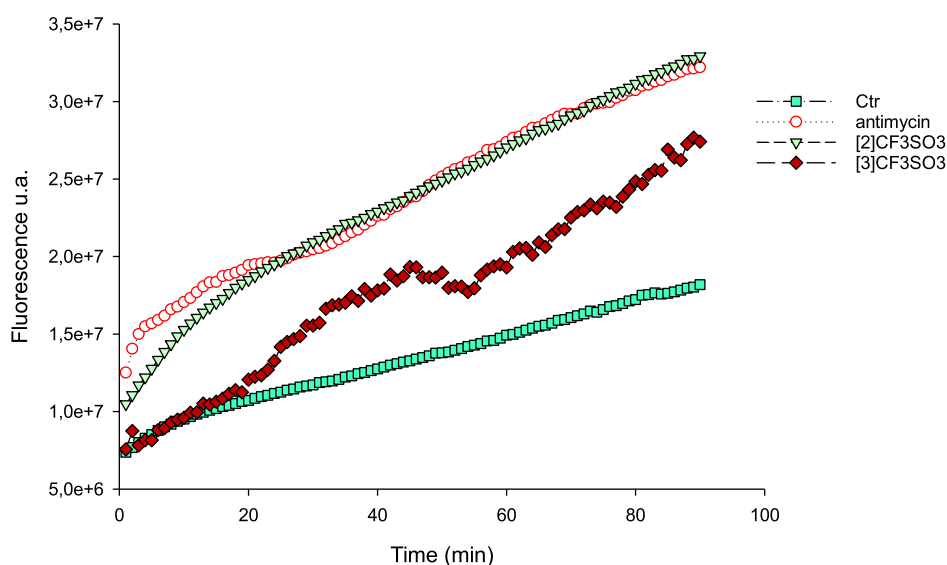


Figure 8. ROS production in U1285 cells. Cells were preincubated in PBS/10 mM glucose medium for 20 min at 37 °C in the presence of 10 μ M CM-H₂DCFDA and then treated with the tested compounds.

inhibitory effect was evaluated by means of the APH test. IC₅₀ values were calculated from the dose–survival curves using a four-parameter logistic model ($p < 0.05$). SD = standard deviation.

Remarkably, the 3D cytotoxicity studies not only confirmed the superior anticancer potential of the ferrocenyl derivative [2]CF₃SO₃ with respect to the phenyl-analogue [3]CF₃SO₃, but also unveiled the higher activity of [2]CF₃SO₃ than the reference drug cisplatin, within a tridimensional environment.

Afterward, we evaluated the ability of [2]CF₃SO₃ and [3]CF₃SO₃ to increase the total basal production of reactive oxygen species (ROS) in U1285 cancer cells. As clearly shown in Figure 8, [2]CF₃SO₃ triggered a substantial time-dependent rise in cellular basal hydrogen peroxide production, similar to the effect induced by antimycin, a well-known inhibitor of mitochondrial Complex III in the respiratory chain. Complex [3]CF₃SO₃ was also effective in enhancing cellular basal ROS production, although to a significantly lower extent.

Overall, previous findings on related diiron complexes as well as the data collected in this study suggest that the triiron complex exerts its antitumor effect by hampering cellular redox homeostasis, possibly disrupting mitochondria, and this activity is enhanced by the presence of the ferrocenyl group.^{23–27}

3. CONCLUDING REMARKS

The ferrocene skeleton possesses distinct properties that have inspired its conjugation with other metal structures, pointing to various applications. Here, we have described the use of CNFc as a ligand for the Fe₂Cp₂(CO)₃ scaffold and its subsequent methylation to generate the first ferrocenyl-decorated aminocarbyne, [2]⁺. Notably, the ferrocenyl substituent provides a stabilizing effect to the aminocarbyne system and the entire cationic complex, which is indefinitely air stable and exhibits a significant robustness in aqueous solutions under pseudophysiological conditions. Spectroscopic data and DFT outcomes highlight that the *N*-ferrocenyl aminocarbyne ligand behaves as a moderate π -acceptor strictly similar to its *N*-phenyl counterpart. In comparison to related diiron complexes, the triiron complex [2]⁺ exhibits a distinct electrochemical behavior, consisting in reduction and oxidation events centered

at the [Fe^IFe^I] core and the Fe^{II} of the ferrocenyl, respectively. Cellular experiments conducted on both the *N*-ferrocenyl, [2]⁺, and *N*-phenyl, [3]⁺, aminocarbyne complexes suggest that the unique combination of electrochemical properties in [2]⁺ is key to its enhanced ability to trigger the production of ROS within cancer cells. It is remarkable that, while [2]⁺ displays an averagely moderate 2D antiproliferative activity against cancer cell lines, its performance in a more reliable 3D model exceeds that of the clinical drug cisplatin. The conjugation of an easily available diiron framework with the ferrocenyl moiety represents a promising strategy with potential implications in drug development.²⁷ Future studies will focus on the modification of [2]⁺, exploiting the arsenal of reactions documented for analogous diiron aminocarbyne complexes,¹⁹ and aiming to produce novel organometallic structures with, hopefully, optimized characteristics and pharmacological profiles.

4. EXPERIMENTAL SECTION

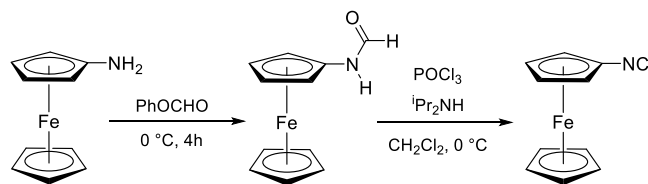
4.1. General Experimental Details. Reactants and solvents were purchased from Alfa Aesar, Merck, Strem, or TCI Chemicals and were of the highest purity available. POCl₃ and Et₃N (over 4 Å MS) were stored under N₂ atmosphere as received. Syntheses were conducted under N₂ atmosphere using standard Schlenk techniques, and products were conserved under N₂ once isolated. Complexes [4,5]CF₃SO₃ were prepared according to the literature.²⁴ Dichloromethane, tetrahydrofuran, and diethyl ether were dried with the solvent purification system mBraun MB SP55, while acetonitrile was distilled from CaH₂ and diisopropylamine from BaO. Chromatography separations were carried out on columns of silica gel (70–230 mesh), neutral alumina, or deactivated alumina (Merck, 4% w/w water) using solvents from the bottle under N₂ flux. IR spectra of solutions were recorded using a CaF₂ liquid transmission cell (1500–2300 cm⁻¹) on a PerkinElmer Spectrum 100 FT-IR spectrometer. IR bands attributed to terminal and bridging CO/CNR ligands are indicated as *t*-CO/*t*-CN and μ -CO/ μ -CN, respectively. UV–vis spectra were recorded on an Ultraspec 2100 Pro spectrophotometer using PMMA cuvettes (1 cm path length). IR and UV–vis spectra were processed with Spectragryph.⁶⁸ NMR spectra were recorded on a Bruker Avance II DRX400 instrument equipped with a BBFO broadband probe. Chemical shifts were referenced to the residual solvent peaks⁶⁹ or external standard (CFCl₃ for ¹⁹F NMR). NMR spectra were assigned with the assistance of ¹H NOESY, ¹H–¹H

COSY, and ^1H - ^{13}C (*gs*-HSQC and *gs*-HMBC) correlation experiments.⁷⁰ NMR signals due to secondary isomeric forms (where it has been possible to detect them) were italicized. Elemental analyses were performed on a Vario MICRO cube instrument (Elementar).

4.2. Optimized Synthesis and Characterization of CNFc and Phenyl Isocyanide.

4.2.1. Isocyanoferrrocene, CNFc (Scheme 3). This synthesis was performed with slight modifications to previously reported procedures.^{37,71,72} Aminoferrrocene was prepared using the procedure described in the Supporting Information (Scheme S1). In a Schlenk tube at 0 °C, phenyl formate (0.76 mL, 7.03 mmol) was added to aminoferrrocene (707 mg, 3.51 mmol), and this mixture was stirred for 4 h. Complete consumption of aminoferrrocene was checked by TLC (eluent: Et₂O). All volatiles were removed under vacuum at 40 °C. The resulting brown oil was dissolved into a hexane/Et₂O mixture, and this solution was passed through a SiO₂ column. Elution with hexane was allowed to remove impurities, and then a bright-orange solution was collected using Et₂O as eluent. Drying under vacuum afforded an orange solid corresponding to ferrocenyl formamide (FcNHCHO). The solid was dissolved in CH₂Cl₂ (18 mL), then POCl₃ (0.33 mL, 3.51 mmol) and anhydrous diisopropylamine (2.48 mL, 17.6 mmol) were added. The resulting solution was stirred at 0 °C, and a color change from orange to brown was noticed along 2 h. After stirring for 6 h, the reaction mixture was quenched with 40 mL of 10% aqueous K₂CO₃. The organic layer was separated and washed twice with 30 mL 10% aqueous K₂CO₃ in air. Volatiles were removed under vacuum. The residue was dissolved in Et₂O/hexane (1:1 v/v), and this solution was passed through a SiO₂ column. Removal of volatiles under vacuum gave the title product a crystalline orange solid. Yield 685 mg, 92%. Anal. Calcd for C₁₁H₉FeN: C, 62.60; H, 4.30; N, 6.64. Found: C, 62.38; H, 4.28; N, 6.84. IR (CH₂Cl₂): $\tilde{\nu}/\text{cm}^{-1}$ = 2149w-sh, 2127s (C≡N). ^1H NMR (CDCl₃): δ/ppm = 4.55 (t, $^3J_{\text{HH}}$ = 2.0 Hz, 2H, C₅H₄); 4.30 (s, 5H, Cp); 4.12 (t, $^3J_{\text{HH}}$ = 2.0 Hz, 2H, C₅H₄).

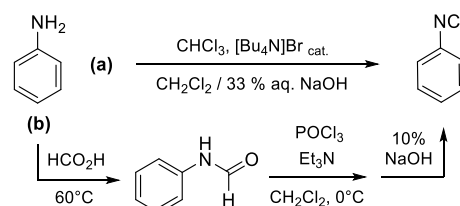
Scheme 3. Two-step Synthesis of CNFc



4.2.2. Phenyl Isocyanide, CNPh (Scheme 4).
4.2.2.1. Hoffman Method.^{73–75} A solution of [Bu₄N]Br (50 mg, 0.15 mmol), aniline (490 mg, 5.3 mmol), and CHCl₃ (0.5 mL, 6 mmol) in CH₂Cl₂ (5 mL) was added under vigorous stirring to a 100 mL tube containing 33% wt aqueous NaOH (2.5 g/5 mL). The biphasic mixture was stirred at ambient temperature overnight. Conversion was checked by IR, then the mixture was diluted with CH₂Cl₂, water, and transferred into a separatory funnel. The aqueous phase was discarded; the organic phase was extracted with saturated NaHCO₃ (×2) and water. Volatiles were removed under vacuum without external heating (*caution! PhNC is toxic, this operation must be performed in a well-ventilated fume hood*), affording an orange-brown oil (yield: 434 mg) that was immediately allowed to react with [Fe₂Cp₂(CO)₄]. Phenyl isocyanide was highly sensitive to these reaction conditions, resulting in a nonreproducible yield and purity. Silica and/or alumina chromatography resulted in its complete degradation.

4.2.2.2. Ugi Method. Phenyl formamide (250 mg, 2.06 mmol), prepared according to an optimized literature method⁷⁶ (see Supporting Information), was dissolved in CH₂Cl₂ (6 mL) and treated with Et₃N (0.60 mL, 4.3 mmol). The pale-yellow solution was cooled to 0 °C, and then POCl₃ (0.20 mL, 2.1 mmol) was added dropwise. The mixture was stirred at 0 °C for 1 h, then allowed to heat to ambient temperature and treated with 10% NaOH (10 mL). The mixture was stirred for 10 min, then diluted with H₂O and moved into a separatory funnel. The aqueous phase was extracted with CH₂Cl₂ (4× 10 mL). The combined organic fractions were taken to

Scheme 4. Preparation of Phenyl Isocyanide from Aniline according to the Hoffman (a) or Ugi (b) Methodologies



dryness under vacuum without external heating (*caution! PhNC is toxic, this operation must be performed in a well-ventilated fume hood*), affording a pale red oil that was immediately allowed to react with [Fe₂Cp₂(CO)₄]. IR (CH₂Cl₂): $\tilde{\nu}/\text{cm}^{-1}$ = 2130s (CN), 1648m-sh, 1626m, 1589m. IR (MeCN): $\tilde{\nu}/\text{cm}^{-1}$ = 2130s (CN), 1649m-sh, 1628m, 1589m. It is essential to perform the reaction below room temperature and to quench the final mixture with NaOH; workups in less basic conditions (e.g., saturated NaHCO₃, 10% Na₂CO₃)^{47–79} resulted in extensive decomposition of the isocyanide.

4.3. Synthesis and Characterization of Diiron Complexes.

4.3.1. [Fe₂Cp₂(CO)₂(μ-CO){μ-CN(Me)(Fc)}]CF₃SO₃, [2]CF₃SO₃ (Figure 9). A solution of [Fe₂Cp₂(CO)₄] (430 mg, 1.21 mmol) in acetonitrile (15 mL) was treated with 1 equiv of freshly synthesized CNFc. The resulting dark-brown solution was stirred at room temperature. After 2 h, a brown precipitate was formed, stirring was prolonged for further 20 h, then volatiles were removed under reduced pressure. The resulting dark-brown solid contains [Fe₂Cp₂(CO)₃(CNFc)], 1, and a minor amount of unreacted [Fe₂Cp₂(CO)₄]. IR (CH₂Cl₂): $\tilde{\nu}/\text{cm}^{-1}$ = 2100w (t-CN), 1988s (t-CO), 1951s (t-CO), 1788m (μ-CO), 1751 (μ-CO), 1691s (μ-CN). IR (CH₃CN): $\tilde{\nu}/\text{cm}^{-1}$ = 2098w (t-CN), 1984s (t-CO), 1946s (t-CO), 1790m (μ-CO), 1753 (μ-CO), 1693s (μ-CN).

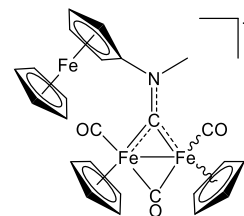


Figure 9. Structure of [2]⁺.

The residue was dissolved in CH₂Cl₂ (15 mL), and methyl triflate (0.13 mL, 1.2 mmol) was added dropwise to the stirred solution. The mixture was stirred at room temperature for 4 h, then it was directly charged on top of a deactivated alumina column (length 6 cm and diameter 3.5 cm). Impurities were removed by using CH₂Cl₂ and CH₂Cl₂/THF (1:1 v/v) as eluents. A bright-red band corresponding to [2]CF₃SO₃ was collected by using neat CH₃CN as eluent. According to ^1H NMR analyses, the eluted mixture was progressively enriched with the *cis* isomer and the final portion of the band contained pure *cis*-[2]CF₃SO₃. Solvent removal under reduced pressure allowed to obtain a red solid, which was washed with Et₂O and dried under vacuum. Yield 744 mg, 88%. Soluble in DMSO, EtOH, CH₂Cl₂, acetone, insoluble in Et₂O. X-ray quality crystals of [2]CF₃SO₃ were obtained CH₂Cl₂/pentane at −20 °C. Anal. Calcd for C₂₆H₂₂F₃Fe₃NO₆S: C, 44.54; H, 3.16; N, 2.00; S, 4.57. Found: C, 44.38; H, 3.21; N, 1.96; S, 4.62. IR (CH₂Cl₂): $\tilde{\nu}/\text{cm}^{-1}$ = 2024 (s, CO); 1992 (w-m, CO); 1837 (m, μ-CO); 1527 (w-m, μ-CN). ^1H NMR (CDCl₃, *cis/trans* ratio = 5): δ/ppm = 5.43, 4.71, 4.64, 4.49, 4.41, 4.32, 4.20 (m, 4H, C₅H₄); 5.36, 5.23, 4.84, 4.64 (s, 10H, Cp); 4.92, 4.89 (s, 3H, Me); 4.56, 4.43 (s, 5H, Cp^{Fc}). $^{13}\text{C}\{^1\text{H}\}$ NMR (CDCl₃): δ/ppm = 326.8 (μ-CN); 255.3 (μ-CO); 209.1, 207.9 (CO); 121.0 (d, $^1J_{\text{CF}}$ = 321 Hz, CF₃); 112.1 (NC^{Cp}); 91.7, 90.53, 90.48 (Cp); 70.8, 70.5 (Cp^{Fc}); 67.7, 67.5, 66.3, 65.6, 65.4, 65.2 (C₅H₄); 60.5, 59.0 (Me). $^{19}\text{F}\{^1\text{H}\}$ NMR (CDCl₃): δ/ppm = −78.1.

4.3.2. [Fe₂Cp₂(CO)₂(μ-CO){μ-CN(Me)(Ph)}]CF₃SO₃, [3]CF₃SO₃ (Figure 10). In a 100 mL round-bottom flask under N₂, freshly prepared PhNC (ca. 2 mmol) was dissolved in anhydrous MeCN (20 mL) and treated with [Fe₂Cp₂(CO)₄] (730 mg, 2.06 mmol). The dark red suspension was stirred at room temperature overnight; a dark violet shade appeared in less than 1 h. Conversion was checked by IR (MeCN), and then volatiles were removed under vacuum. The dark violet residue was suspended in Et₂O and treated with 48% aq HBF₄ (0.3 mL, 2.3 mmol), affording a scarlet red solid. The suspension was stirred for 2 h then moved on top of an alumina column (h 5 d 3.4 cm). A dark red band containing [Fe₂Cp₂(CO)₄] and other impurities was eluted using Et₂O, then a dark violet band was eluted using a 5% Et₃N solution in CH₂Cl₂ (ca. 200 mL). Volatiles were removed under vacuum, affording a dark violet residue containing [Fe₂Cp₂(CO)₂(μ-CO)(μ-CNPh)]⁸⁰ {IR (CH₂Cl₂): $\tilde{\nu}/\text{cm}^{-1}$ = 1991s (t-CO), 1951s (t-CO), 1781m (μ-CO), 1691s (μ-CN)} and a minor amount of [Fe₂Cp₂(CO)(CNPh)(μ-CO)(μ-CNPh)]⁵² {IR (CH₂Cl₂): $\tilde{\nu}/\text{cm}^{-1}$ = 2093s (t-CN)}. The solid (ca. 0.8 mmol) was dissolved in anhydrous CH₂Cl₂ (15 mL), and methyl triflate (0.10 mL, 0.91 mmol) was added dropwise under stirring. The dark violet solution rapidly changed to dark red and was stirred at room temperature for 4 h. Next, the mixture was moved on top of an alumina column (h 4.5, d 4.5 cm). Impurities were eluted with CH₂Cl₂, CH₂Cl₂/THF 1:1 v/v, and THF, then a red band was eluted with MeCN (ca. 200 mL). Volatiles were removed under vacuum. The residue was dissolved in CH₂Cl₂ and filtered over a Celite pad. The filtrate solution was taken to dryness under vacuum, affording a red foamy solid that was washed with hexane, dried under vacuum (40 °C), and stored under N₂. Yield: 194 mg, ca. 41%. Soluble in CH₂Cl₂, acetone, EtOH, and DMSO, scarcely soluble in Et₂O, toluene, insoluble in water. Anal. Calcd for C₂₂H₁₈F₃Fe₂NO₆S: C, 44.55; H, 3.06; N, 2.36; S, 5.41. Found: C, 44.78; H, 3.20; N, 2.55; S, 5.24. IR (CH₂Cl₂): $\tilde{\nu}/\text{cm}^{-1}$ = 2025s (CO), 1993w-sh (CO), 1839m (μ-CO), 1549m, 1531w-sh (CN). ¹H NMR (CDCl₃): δ/ppm = 7.76 (br, 2H, Ph^{ortho}); 7.62 (t, ³J_{HH} = 7.5 Hz, 2H, Ph^{meta}); 7.54 (t, ³J_{HH} = 7.3 Hz, 1H, Ph^{para}); 5.43 (s, 5H, Cp); 4.72 (s, 5H, Cp'); 4.55 (s, 3H, Me). ¹³C{¹H} NMR (CDCl₃): δ/ppm = 324.5 (μ-CN); 254.4 (μ-CO); 208.8, 207.7 (CO); 150.6 (Ph^{ipso}); 130.7 (Ph^{ortho}); 129.6 (Ph^{meta}); 125.3 (Ph^{para}); 120.9 (d, ¹J_{CF} = 309 Hz, CF₃); 90.5, 90.2 (Cp); 57.3 (Me). ¹⁹F{¹H} NMR (CDCl₃): δ/ppm = -78.0. The isolated compound contains ca. 7% mol. of [Fe₂Cp₂(CO)(CNPh)(μ-CO){μ-CN(Me)(Ph)}]CF₃SO₃. ¹H NMR (CDCl₃): δ/ppm = 7.48 (m), 7.10 (d) (Ph); 5.34 (s, 5H, Cp); 4.69 (s, 5H, Cp'); 4.55 (s, 3H, NMe). IR (CH₂Cl₂): $\tilde{\nu}/\text{cm}^{-1}$ = 2127 (t-CN), 1773 (μ-CO).

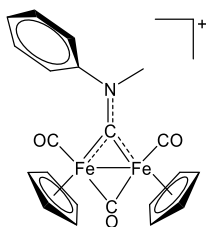


Figure 10. Structure of [3]⁺.

4.4. Isomerization Reactions of [2]CF₃SO₃. General procedure: Complex [2]CF₃SO₃ (ca. 15 mg) was heated at reflux under N₂ in selected solvents for several hours, then the solvent was removed under vacuum, and the residue was analyzed by ¹H NMR (CDCl₃ solution). Thermal treatment in isopropanol, acetonitrile, methanol, or toluene (1–4 h) did not affect the isomeric ratio. Refluxing in DMF resulted in extensive degradation. Conditions leading to an increased isomeric ratio are reported in Table S. Variable byproduct formation and/or degradation were observed, generally more pronounced as the isomeric ratio increased.

4.5. Electrochemistry. CV measurements were performed with a PalmSens4 instrument interfaced to a computer employing PSTrace5 electrochemical software. Anhydrous CH₂Cl₂ (Merck) and THF

Table 5. Experimental Conditions and Resulting Isomeric Ratios (Evaluated by Subsequent ¹H NMR Spectra) Related to [2]CF₃SO₃

solvent, time, temperature	cis/trans ratio
EtOH, 4 h, reflux	6
EtOH, 7 h, reflux	8
acetone, 2.5 h, reflux	18
DMF, 4 h, 110 °C	9
DMF, overnight, 110 °C	17

(Merck) were stored under argon over 3 Å molecular sieves. [NⁿBu₄]PF₆ (Fluka, electrochemical grade) and FeCp₂ (Fluka) were used without further purification. CV measurements were carried out under argon using 0.2 M [NⁿBu₄]PF₆ in CH₂Cl₂ or THF as the supporting electrolyte. The working and the counter electrodes consisted of a Pt disk and a Pt gauze, respectively. A leakless miniature Ag/AgCl/KCl (3.4 mol/L) electrode (eDAQ) was employed as a reference. The three-electrode home-built cell was predried by heating under vacuum and filled with argon. The Schlenk-type construction of the cell maintained anhydrous and anaerobic conditions. The solution of the supporting electrolyte, prepared under argon, was introduced into the cell, and the CV of the solvent was recorded. The analyte was then introduced, and voltammograms were recorded; lastly, a small amount of ferrocene was added, and the CV was repeated. Under the present experimental conditions, the one-electron oxidation of ferrocene occurred at E° = +0.45 V vs Ag/AgCl in CH₂Cl₂, and at E° = +0.57 V vs Ag/AgCl in THF.

PB solution (Na₂HPO₄/KH₂PO₄, Σc_(PO₄) = 50 mM, pH = 7.3) was prepared in ultrapure H₂O and used as an aqueous supporting electrolyte. The three-electrode home-built cell was equipped with a Pt sheet counter electrode, a Teflon-encapsulated glassy-carbon (GC) working electrode (BASi, ø 3 mm), and a leak-free Ag/AgCl/KCl (3.4 mol/L) reference electrode (eDAQ). Prior to measurements, the working GC electrode was polished by the following procedure:⁸¹ manual rubbing with 0.3 μM Al₂O₃ slurry in water (eDAQ) for 2 min, then sonication in ultrapure water for 10 min, manual rubbing with 0.05 μM Al₂O₃ slurry in water (eDAQ) for 2 min, then sonication in ultrapure water for 10 min. The PB (5.0 mL) was introduced into the cell, deaerated by argon bubbling for some minutes, and the CV of the solvent recorded. The analyte was then introduced, and voltammograms were recorded (scan rate: 0.1 V/s). Under the present experimental conditions, the one-electron reduction of ferricinium in the PB occurred at E° = +0.20 V vs Ag/AgCl.

Controlled potential coulometry was performed in an H-shaped cell with anodic and cathodic compartments separated by a sintered-glass disk. The working macroelectrode and counter-electrode were platinum gauze.

IR SEC measurements were carried out using an OTTLE cell equipped with CaF₂ windows, platinum mini-grid working and auxiliary electrodes, and a silver wire pseudoreference electrode.⁵⁷ During the microelectrolysis procedures, the electrode potential was controlled by a PalmSens4 instrument interfaced to a computer employing PSTrace5 electrochemical software. Argon-saturated CH₂Cl₂ or THF/[NⁿBu₄]PF₆ 0.2 M solutions of the analyzed compound were used. The in situ SEC experiments were performed by collecting IR spectra at fixed time intervals during oxidation or reduction, obtained by continuously increasing or lowering the initial working potential at a scan rate of 1.0 or 2.0 mV s⁻¹, or by electrolysis at constant potential. In this second procedure, during the electrolysis, the IR spectra were collected each 30 s.

4.6. DFT Calculations. Geometry optimizations were performed using the PBEh-3c method, which is a reparametrized version of PBE0⁸² (with 42% HF exchange) that uses a split-valence double-ζ basis set (def2-mSVP)^{83,84} and adds three corrections considering dispersion, basis set superposition, and other basis set incompleteness effects.^{85–87} The C-PCM implicit solvation model was added to PBEh-3c calculations.^{88,89} IR simulations were carried out using the harmonic approximation, from which zero-point vibrational energies

and thermal corrections ($T = 298.15$ K) were obtained.⁹⁰ The software used was ORCA version 5.0.3.⁹¹ The output was elaborated using MultiWFN, version 3.8.⁹² The cartesian coordinates of the DFT-optimized structures were collected in a separated.xyz file.

4.8. Behavior in Aqueous Solutions. **4.8.1. Solubility in D₂O.** The selected diiron complex was suspended in a D₂O solution (0.7 mL) containing dimethyl sulfone (Me₂SO₂; 4.5×10^{-3} M), and this suspension was stirred at room temperature (21 ± 1 °C) for 3 h. The saturated solution was filtered over Celite and analyzed by ¹H NMR (delay time = 3 s; number of scans = 20). The concentration (=solubility) was calculated as the relative integral with respect to Me₂SO₂ as an internal standard [$\delta/\text{ppm} = 3.14$ (s, 6H)] (Table 2). NMR data are reported in the Supporting Information.

4.8.2. Octanol/Water Partition Coefficient (Log P_{ow}). Partition coefficients (P_{ow}), defined as $P_{ow} = c_{org}/c_{aq}$ where c_{org} and c_{aq} were the molar concentrations of the selected compound in the *n*-octanol and aqueous phases, respectively, were determined by the shake-flask method and UV–vis measurements, according to a previously described procedure.^{93,94} All operations were carried out at room temperature (21 ± 1 °C). The stock solution of [2]CF₃SO₃ was prepared in water-saturated octanol, while the stock solution of [2]CF₃SO₃ in octanol-saturated water. The wavelength corresponding to a well-defined maximum of shoulder absorption of each compound (320–400 nm range) was used for UV–vis quantitation. The procedure was repeated three times on each sample (from the same stock solution); the results are given as the mean \pm standard deviation (Table 2).

4.8.3. Stability in CD₃OD/D₂O Mixture. The selected diiron complex (ca. 5 mg) was dissolved in CD₃OD/D₂O (5:2 v/v, ca. 0.7 mL) containing 4.03×10^{-3} M dimethylsulfone (Me₂SO₂) as an internal standard. This solution was filtered over Celite, then transferred into an NMR tube, and the ¹H NMR spectrum was recorded. The mixture was maintained at 37 °C for 48 h. After filtration over Celite, the solution was analyzed by ¹H NMR. The residual amount of starting material in the final solution (with respect to the initial spectrum) was calculated as the relative integral with respect to Me₂SO₂ as an internal standard. NMR spectra were recorded using the following settings: number of scans = 20; relaxation delay = 3 s [2]CF₃SO₃. ¹H NMR (D₂O/CD₃OD 5:2 v/v): $\delta/\text{ppm} = 5.38, 5.31$ (s, 5H); 4.94 (s, *), 4.80 (s, *), 4.78 (s, *); 4.60 (s), 4.57–4.54 (m), 4.51 (s) (7H); cis/trans ratio ca. 1. *Over HDO peak. [3]CF₃SO₃. ¹H NMR (D₂O): $\delta/\text{ppm} = 7.74$ –7.62 (m, 5H), 5.44 (s, 5H), 4.55 (s, 3H). Cp' is hidden by the HDO peak. ¹H NMR (D₂O/CD₃OD 5:2 v/v): $\delta/\text{ppm} = 7.85$ –7.59 (m, 5H), 5.46 (s, 5H), 4.78 (s), 4.56 (s, 3H).

4.8.4. Stability in CD₃OD/DMEM Mixture. Deuterated cell culture medium (DMEM-d) was prepared by dissolving powdered DMEM cell culture medium (1000 mg/L glucose and L-glutamine, without sodium bicarbonate and phenol red; D2902-Sigma-Aldrich) in D₂O (10 mg/mL, according to the manufacturer's instructions). The solution was treated with Me₂SO₂ (ca. 6×10^{-3} M), NaH₂PO₄, and Na₂HPO₄ (25 mM total phosphate, pD = 7.4),⁹⁵ then stored under N₂. Solutions of diiron complexes in a DMEM-d/CD₃OD 5:2 v/v mixture were prepared and treated as described above. The residual amount of starting material in solution after 24 h at 37 °C was calculated with respect to Me₂SO₂ as an internal standard (Table 2).

4.9. Biological Studies. **4.9.1. Cytotoxicity.** The tested complexes were dissolved in the minimum DMSO amount prior to cell culture testing. A calculated amount of the stock drug DMSO solution was added to the cell culture media to reach a final maximum DMSO concentration of 0.5%, which had no effects on cell viability. Cisplatin was dissolved in a 0.9% sodium chloride solution. MTT [3-(4,5-dimethylthiazol-2-yl)-2,5-diphenyltetrazolium bromide], cisplatin, and ImmunoPure *p*-nitrophenyl phosphate (APH) were obtained from Sigma Chemical Co., St. Louis, USA.

4.9.2. Cell Cultures. Human colon (HCT-15) and pancreatic (PSN-1) carcinoma cell lines, along with human SCLC (U1285), were obtained from the American Type Culture Collection (ATCC, Rockville, MD). Human ovarian 2008 cancer cells were kindly provided by Prof. G. Marverti (Dept. of Biomedical Science of

Modena University, Italy). Human cervical A431 cancer cells were kindly provided by Prof. P. Perego (Fondazione IRCCS Istituto Nazionale Tumori, Milan, Italy).

Cell lines were maintained in the logarithmic phase at 37 °C in a 5% carbon dioxide atmosphere using RPMI-1640 culture medium containing 10% fetal calf serum (Euroclone, Milan, Italy), antibiotics (50 units/mL penicillin and 50 $\mu\text{g}/\text{mL}$ streptomycin), and 2 mM L-glutamine.

4.9.3. Spheroid Cultures. Spheroid cultures were obtained by seeding 2.5×10^3 cells/well in a round-bottom nontissue culture-treated 96 well-plate (Greiner Bio-one, Kremsmünster, Austria) in phenol red free RPMI-1640 medium (Sigma Chemical Co.), containing 10% FCS and supplemented with 20% methyl cellulose stock solution.

4.9.4. MTT Assay. The growth inhibitory effect toward tumor cells was evaluated by means of an MTT assay, as previously described.⁹⁶ IC₅₀ values were calculated with a four-parameter logistic (4-PL) model. All the values were the means \pm SD of not less than four independent experiments.

4.9.5. Acid Phosphatase Assay. An APH-modified assay was used for determining cell viability in 3D spheroids, as previously described.⁹⁷ IC₅₀ values were calculated with a four-parameter logistic (4-PL) model. All the values are the means \pm SD of not less than four independent experiments.

4.9.6. ROS Production. The production of ROS was measured in U1285 cells (10^4 per well) grown for 24 h in a 96-well plate in RPMI medium without phenol red (Sigma Chemical Co.). Cells were then washed with PBS and loaded with 10 μM 5-(and-6)-chloromethyl-2',7'-dichlorodihydrofluorescein diacetate acetyl ester (CM-H₂DCFDA) (Molecular Probes-Invitrogen, Eugene, OR) for 25 min, in the dark. Afterward, cells were washed with PBS and incubated with increasing concentrations of the tested compounds. Fluorescence increase was estimated utilizing the wavelengths of 485 nm (excitation) and 527 nm (emission) in a VICTOR X3 (PerkinElmer, USA) plate reader. Antimycin (3 μM , Sigma Chemical Co.), a potent inhibitor of Complex III in the electron transport chain, was used as a positive control.

■ ASSOCIATED CONTENT

Supporting Information

The Supporting Information is available free of charge at <https://pubs.acs.org/doi/10.1021/acs.inorgchem.3c03408>.

Synthesis/characterization of CNF_c; IR and NMR spectra; computational results; spectroelectrochemical studies (PDF)

Cartesian coordinates of the DFT-optimized structures (XYZ)

■ AUTHOR INFORMATION

Corresponding Author

Fabio Marchetti – Department of Chemistry and Industrial Chemistry, University of Pisa, I-56124 Pisa, Italy;

orcid.org/0000-0002-3683-8708;

Email: fabio.marchetti@unipi.it; https://people.unipi.it/fabio_marchetti/

Authors

Chiara Saviozzi – Department of Chemistry and Industrial Chemistry, University of Pisa, I-56124 Pisa, Italy;

orcid.org/0000-0002-2538-3058

Lorenzo Biancalana – Department of Chemistry and Industrial Chemistry, University of Pisa, I-56124 Pisa, Italy;

orcid.org/0000-0002-9276-0095

Tiziana Funaioli – Department of Chemistry and Industrial Chemistry, University of Pisa, I-56124 Pisa, Italy

Marco Bortoluzzi – Department of Molecular Science and Nanosystems, University of Venezia “Ca’ Foscari”, I-30170 Mestre (VE), Italy; orcid.org/0000-0002-4259-1027

Michele De Franco – Department of Pharmaceutical and Pharmacological Sciences, University of Padova, I-35131 Padova, Italy

Massimo Guelfi – Department of Chemistry and Industrial Chemistry, University of Pisa, I-56124 Pisa, Italy

Valentina Gandin – Department of Pharmaceutical and Pharmacological Sciences, University of Padova, I-35131 Padova, Italy

Complete contact information is available at:

<https://pubs.acs.org/10.1021/acs.inorgchem.3c03408>

Notes

The authors declare no competing financial interest.

ACKNOWLEDGMENTS

L.B. and F.M. acknowledge the financial support from the University of Pisa (Fondi di Ateneo 2020).

REFERENCES

- (1) Astruc, D. Why is Ferrocene so Exceptional? *Eur. J. Inorg. Chem.* **2017**, *2017*, 6–29.
- (2) Astruc, D. From sandwich complexes to dendrimers: journey toward applications to sensing, molecular electronics, materials science, and biomedicine. *Chem. Commun.* **2023**, *59*, 7321–7345.
- (3) Štěpnička, P. Forever young: the first seventy years of ferrocene. *Dalton Trans.* **2022**, *51*, 8085–8102.
- (4) van Staveren, D. R.; Metzler-Nolte, N. Bioorganometallic Chemistry of Ferrocene. *Chem. Rev.* **2004**, *104*, 5931–5986.
- (5) Patra, M.; Gasser, G. The medicinal chemistry of ferrocene and its derivatives. *Nat. Rev. Chem.* **2017**, *1*, 0066.
- (6) Boros, E.; Dyson, P. J.; Gasser, G. Classification of Metal-Based Drugs according to Their Mechanisms of Action. *Chem* **2020**, *6*, 41–60.
- (7) Anthony, E. J.; Bolitho, E. M.; Bridgewater, H. E.; Carter, O. W. L.; Donnelly, J. M.; Imberti, C.; Lant, E. C.; Lermyte, F.; Needham, R. J.; Palau, M.; Sadler, P. J.; Shi, H.; Wang, F.-X.; Zhang, W.-Y.; Zhang, Z. Metallo drugs are unique: opportunities and challenges of discovery and development. *Chem. Sci.* **2020**, *11*, 12888–12917.
- (8) Atkinson, R. C. J.; Gibson, V. C.; Long, N. J. The syntheses and catalytic applications of unsymmetrical ferrocene ligands. *Chem. Soc. Rev.* **2004**, *33*, 313–328.
- (9) Gómez Arrayás, R.; Adrio, J.; Carretero, J. C. Recent Applications of Chiral Ferrocene Ligands in Asymmetric Catalysis. *Angew. Chem., Int. Ed.* **2006**, *45*, 7674–7715.
- (10) Mu, C.; Chang, S. W.; Prosser, K. E.; Leung, A. W. Y.; Santacruz, S.; Jang, T.; Thompson, J. R.; Yapp, D. T. T.; Warren, J. J.; Bally, M. B.; Beischlag, T. V.; Walsby, C. J. Induction of Cytotoxicity in Pyridine Analogues of the Antimetastatic Ru(III) Complex NAMI - A by Ferrocene Functionalization. *Inorg. Chem.* **2016**, *55*, 177–190.
- (11) Gadre, S.; Manikandan, M.; Duari, P.; Chhatar, S.; Sharma, A.; Khatri, S.; Kode, J.; Barkume, M.; Kasinathan, N. K.; Nagare, M.; Patkar, M.; Ingle, A.; Kumar, M.; Kolthur-Seetharam, U.; Patra, M. A Rationally Designed Bimetallic Platinum (II)-Ferrocene Antitumor Agent Induces Non-Apoptotic Cell Death and Exerts in Vivo Efficacy. *Chem.—Eur. J.* **2022**, *28*, No. e202201259.
- (12) López-Hernández, J. E.; Contel, M. Promising heterometallic compounds as anticancer agents: Recent studies in vivo. *Curr. Opin. Chem. Biol.* **2023**, *72*, 102250.
- (13) Mu, C.; Prosser, K. E.; Harrypersad, S.; MacNeil, G. A.; Panchmatia, R.; Thompson, J. R.; Sinha, S.; Warren, J. J.; Walsby, C. J. Activation by Oxidation: Ferrocene-Functionalized Ru(II)-Arene Complexes with Anticancer, Antibacterial, and Antioxidant Properties. *Inorg. Chem.* **2018**, *57*, 15247–15261.
- (14) Shubhankar Gadre, M. M.; Gadre, S.; Chhatar, S.; Chakraborty, G.; Ahmed, N.; Patra, C.; Patra, M. Potent Ruthenium-Ferrocene Bimetallic Antitumor Antiangiogenic Agent That Circumvents Platinum Resistance: From Synthesis and Mechanistic Studies to In Vivo Evaluation in Zebrafish. *J. Med. Chem.* **2022**, *65*, 16353–16371.
- (15) Tauchman, J.; Süß-Fink, G.; Stepnicka, P.; Zava, O.; Dyson, P. J. Arene ruthenium complexes with phosphinoferrrocene amino acid conjugates: Synthesis, characterization and cytotoxicity. *J. Organomet. Chem.* **2013**, *723*, 233.
- (16) Carter, C.; Kratish, Y.; Jurca, T.; Gao, Y.; Marks, T. J. Bis-Ferrocenyl-Pyridinediimine Trinuclear Mixed-Valent Complexes with Metal-Binding Dependent Electronic Coupling: Synthesis, Structures, and Redox-Spectroscopic Characterization. *J. Am. Chem. Soc.* **2020**, *142*, 18715–18729.
- (17) Buday, P.; Celeda, M.; Görls, H.; Mlostóń, G.; Weigand, W. A Remarkable Ring Opening Observed in the Reaction of Cyclopropyl Ferrocenyl Thioketone with Triiron Dodecacarbonyl Fe₃(CO)₁₂. *Eur. J. Inorg. Chem.* **2022**, *2022*, No. e202200520.
- (18) Camara, J. M.; Rauchfuss, T. B. Combining acid-base, redox and substrate binding functionalities to give a complete model for the [FeFe]-hydrogenase. *Nat. Chem.* **2012**, *4*, 26–30.
- (19) Marchetti, F. Constructing Organometallic Architectures from Aminoalkylidene Diiron Complexes. *Eur. J. Inorg. Chem.* **2018**, *2018*, 3987–4003.
- (20) Ritleng, V.; Chetcuti, M. J. Hydrocarbyl Ligand Transformations on Heterobimetallic Complexes. *Chem. Rev.* **2007**, *107*, 797–858.
- (21) van Beek, C. B.; van Leest, N. P.; Lutz, M.; de Vos, S. D.; Klein Gebbink, R. J. M.; de Bruin, B.; Broere, D. L. J. Combining metal-metal cooperativity, metal-ligand cooperativity and chemical non-innocence in diiron carbonyl complexes. *Chem. Sci.* **2022**, *13*, 2094–2104.
- (22) Biancalana, L.; Marchetti, F. Aminocarbyne ligands in organometallic chemistry. *Coord. Chem. Rev.* **2021**, *449*, 214203.
- (23) Agonigi, G.; Biancalana, L.; Lupo, M. G.; Montopoli, M.; Ferri, N.; Zacchini, S.; Binacchi, F.; Biver, T.; Campanella, B.; Pampaloni, G.; Zanotti, V.; Marchetti, F. Exploring the Anticancer Potential of Diiron Bis-cyclopentadienyl Complexes with Bridging Hydrocarbyl Ligands: Behavior in Aqueous Media and In Vitro Cytotoxicity. *Organometallics* **2020**, *39*, 645–657.
- (24) Biancalana, L.; De Franco, M.; Ciancaleoni, G.; Zacchini, S.; Pampaloni, G.; Gandin, V.; Marchetti, F. Easily Available, Amphiphilic Diiron Cyclopentadienyl Complexes Exhibit in vitro Anticancer Activity in 2D and 3D Human Cancer Cells through Redox Modulation Triggered by CO Release. *Chem.—Eur. J.* **2021**, *27*, 10169–10185.
- (25) Campanella, B.; Braccini, S.; Bresciani, G.; De Franco, M.; Gandin, V.; Chiellini, F.; Pratesi, A.; Pampaloni, G.; Biancalana, L.; Marchetti, F. The choice of μ -vinyliminium ligand substituents is key to optimize the antiproliferative activity of related diiron complexes. *Metallomics* **2023**, *15*, mfac096.
- (26) Rocco, D.; Batchelor, L. K.; Agonigi, G.; Braccini, S.; Chiellini, F.; Schoch, S.; Biver, T.; Funaioli, T.; Zacchini, S.; Biancalana, L.; Ruggeri, M.; Pampaloni, G.; Dyson, P. J.; Marchetti, F. Anticancer potential of diiron vinyliminium complexes. *Chem.—Eur. J.* **2019**, *25*, 14739–14816.
- (27) Bresciani, G.; Cervinka, J.; Kostrhunova, H.; Biancalana, L.; Bortoluzzi, M.; Pampaloni, G.; Novohradsky, V.; Brabec, V.; Marchetti, F.; Kasparkova, J. N-Indolyl diiron vinyliminium complexes exhibit antiproliferative effects in cancer cells associated with disruption of mitochondrial homeostasis, ROS scavenging, and antioxidant activity. *Chem.-Biol. Interact.* **2023**, *385*, 110742.
- (28) Schoch, S.; Braccini, S.; Biancalana, L.; Pratesi, A.; Funaioli, T.; Zacchini, S.; Pampaloni, G.; Chiellini, F.; Marchetti, F. When ferrocene and diiron organometallics meet: triiron vinyliminium complexes exhibit strong cytotoxicity and cancer cell selectivity. *Inorg. Chem. Front.* **2022**, *9*, 5118–5139.
- (29) According to IUPAC, metal complexes comprising a carbyne ligand should be called “alkylidene” complexes. See: KreibI, F. R.

Transition Metal Carbyne Complexes; Springer, 1993. However, the term “aminocarbyne” is more familiar in the literature than “aminoalkylidyne”, and the former will be preferentially used throughout this manuscript.

(30) Willis, S.; Manning, A. R. Reactions of $[\text{Fe}_2(\eta\text{-C}_5\text{H}_5)_2(\text{CO})_{4+n}(\text{CNR})_n]$ ($n = 1$ or 2 ; $R = \text{Me}$, Et , or CH_2Ph) with acetyl and benzoyl chlorides. *J. Chem. Soc., Dalton Trans.* **1981**, 322–324.

(31) Complexes $[\text{Fe}_2\text{Cp}_2(\text{CO})_2(\mu\text{-CO})\{\mu\text{-CN}(\text{Me})(\text{R})\}]\text{CF}_3\text{SO}_3$ ($R = \text{tBu}$, $4\text{-C}_6\text{H}_4\text{CN}$) largely decompose upon passing through an alumina column; using a procedure analogous to that illustrated in Scheme 1, the formation of complexes with $R = 2,6\text{-C}_6\text{H}_4\text{F}_2$ and $R = \text{CH}_2\text{SO}_2(4\text{-C}_6\text{H}_4\text{Me})$ did not occur, even when the CO-substitution step was conducted at reflux temperature.

(32) Pombeiro, A. J. L.; Guedes da Silva, M. F. C.; Michelin, R. A. Aminocarbyne complexes derived from isocyanides activated towards electrophilic addition. *Coord. Chem. Rev.* **2001**, 218, 43–74.

(33) Biancalana, L.; Ciancaleoni, G.; Zacchini, S.; Pampaloni, G.; Marchetti, F. Carbonyl-isocyanide mono-substitution in $[\text{Fe}_2\text{Cp}_2(\text{CO})_4]$: A re-visitation. *Inorg. Chim. Acta* **2021**, 517, 120181 and references therein.

(34) Barybin, M. V. Nonbenzenoid aromatic isocyanides: New coordination building blocks for organometallic and surface chemistry. *Coord. Chem. Rev.* **2010**, 254, 1240–1252.

(35) Nemykin, V. N.; Dudkin, S. V.; Fathi-Rasekh, M.; Spaeth, A. D.; Rhoda, H. M.; Belosludov, R. V.; Barybin, M. V. Probing Electronic Communications in Heterotrinary Fe - Ru - Fe Molecular Wires Formed by Ruthenium(II) Tetraphenylporphyrin and Isocyanoferrrocene or 1,1'-Diisocyanoferrrocene Ligands. *Inorg. Chem.* **2015**, 54, 10711–10724.

(36) Nemykin, V. N.; Purchel, A. A.; Spaeth, A. D.; Barybin, M. V. Probing the Electronic Properties of a Trinuclear Molecular Wire Involving Isocyanoferrrocene and Iron(II) Phthalocyanine Motifs. *Inorg. Chem.* **2013**, 52, 11004–11012.

(37) Huang, Y.-C.; Lan, W.-Y.; Ching, W.-M.; Hsu, S. C. N. Formation of iron(III)-thiolate metallocyclophane using a ferrocene-based bis-isocyanide. *New J. Chem.* **2020**, 44, 18242–18249.

(38) Barybin, M. V.; Holovics, T. C.; Deplazes, S. F.; Lushington, G. H.; Powell, D. R.; Toriyama, M. First Homoleptic Complexes of Isocyanoferrrocene. *J. Am. Chem. Soc.* **2002**, 124, 13668–13669.

(39) Vosahlo, P.; Franc, M.; Harmach, P.; Schulz, J.; Stepnicka, P. Synthesis of gold(I) diaminocarbyne complexes by the addition of amines across coordinated isocyanoferrrocene. *J. Organomet. Chem.* **2023**, 1001, 122843.

(40) Mahmudov, K. T.; Kukushkin, V. Y.; Gurbanov, A. V.; Kinzhalov, M. A.; Boyarskiy, V. P.; da Silva, M. F. C. G.; Pombeiro, A. J. L. RETRACTED: Isocyanide metal complexes in catalysis. *Coord. Chem. Rev.* **2019**, 384, 65–89.

(41) Boyarskiy, V. P.; Bokach, N. A.; Luzyanin, K. V.; Kukushkin, V. Y. Metal-Mediated and Metal-Catalyzed Reactions of Isocyanides. *Chem. Rev.* **2015**, 115, 2698–2779.

(42) Biancalana, L.; Fiaschi, M.; Ciancaleoni, G.; Pampaloni, G.; Zanotti, V.; Zacchini, S.; Marchetti, F. A comparative structural and spectroscopic study of diiron and diruthenium isocyanide and aminocarbyne complexes. *Inorg. Chim. Acta* **2022**, 536, 120886.

(43) GuilleVIC, M. A.; Hancox, E. L.; Mann, B. E. A Reinvestigation of the Solution Structure and Dynamics of $[\text{Fe}_2(\eta\text{-C}_5\text{H}_5)_2(\text{CO})_{4+n}(\text{CNMe})_n]$, $n = 1$ or 2 . *J. Chem. Soc., Dalton Trans.* **1992**, 1729–1733.

(44) Farrugia, L. J. Dynamics and fluxionality in metal carbonyl clusters: some old and new problems. *J. Chem. Soc., Dalton Trans.* **1997**, 11, 1783–1792.

(45) Howell, J. A. S.; Rowan, A. J. Synthesis and fluxional character of complexes of the type $[\text{M}_2(\text{cp})_2(\text{CO})_3(\text{CNR})]$ ($\text{M} = \text{Fe}$ or Ru , $\text{cp} = \eta\text{-C}_5\text{H}_5$). *J. Chem. Soc., Dalton Trans.* **1980**, 3, 503–510.

(46) Burrows, A. D.; Fleischer, H.; Michael, D.; Mingos, P. The synthesis and structural characterization of a pentapalladium cluster, $[\text{Pd}_5(\mu\text{-SO}_2)_3(\mu\text{-CNXyl})_2(\text{CNXyl})_5]$, with linear bridging isocyanide ligands. *J. Organomet. Chem.* **1992**, 433, 311–321.

(47) Agonigi, G.; Bortoluzzi, M.; Marchetti, F.; Pampaloni, G.; Zacchini, S.; Zanotti, V. Regioselective Nucleophilic Additions to Diiron Carbonyl Complexes Containing a Bridging Aminocarbyne Ligand: A Synthetic, Crystallographic and DFT Study. *Eur. J. Inorg. Chem.* **2018**, 2018, 960–971.

(48) Cox, G.; Dowling, C.; Manning, A. R.; McArdle, P.; Cunningham, D. A reinvestigation of the reaction of $[\text{Fe}_2(\eta\text{-C}_5\text{H}_5)_2(\text{CO})_{4+n}(\text{CNR})_n]$ ($n = 1$ or 2) with strong alkylating agents. *J. Organomet. Chem.* **1992**, 438, 143–158.

(49) Pombeiro, A. J. L. Electron-donor/acceptor properties of carbynes, carbenes, vinylidenes, allenylidenes and alkynyls as measured by electrochemical ligand parameters. *J. Organomet. Chem.* **2005**, 690, 6021–6040.

(50) Bresciani, G.; Zacchini, S.; Pampaloni, G.; Bortoluzzi, M.; Marchetti, F. Diiron Aminocarbyne Complexes with NCE⁻ Ligands ($E = \text{O}$, S , Se). *Molecules* **2023**, 28, 3251.

(51) Hu, H.; Ichiryu, H.; Nakajima, K.; Ogasawara, M. Estimating Effective Steric and Electronic Impacts of a Ferrocenyl Group in Organophosphines. *ACS Omega* **2021**, 6, 5981–5989.

(52) Hill, A. F.; Manzano, R. A. A $[\text{C}_1 + \text{C}_2]$ route to propargylidyne complexes. *Dalton Trans.* **2019**, 48, 6596–6610.

(53) Howell, J. A. S.; Mays, M. J.; Hunt, I. D.; Mills, O. S. The preparation and structural characterization of trans-anti- $(\eta^5\text{-C}_5\text{H}_5)_2\text{Fe}_2(\text{CO})_2(\text{PhNC})_2$. *J. Organomet. Chem.* **1977**, 128, C29–C30.

(54) Manning, A. R.; McNally, G.; Soye, P. The preparation and spectra of $[\text{Fe}_2(\eta\text{-C}_5\text{H}_5)_2(\text{CO})_{4+n}(\text{CNAr})_n]$ complexes. The reaction of $[\text{Fe}(\text{CO})_5\text{-m}(\text{CNAr})_m]$ with dicyclopentadiene. *Inorg. Chim. Acta* **1991**, 180, 103–110.

(55) Joshi, K. K.; Mills, O. S.; Pauson, P. L.; Shaw, B. W.; Stubbs, W. H. An Iron Complex with a Bridging Isonitrile Group. *Chem. Commun.* **1965**, 10, 181–182.

(56) Christian, G.; Lentz, D.; Hartl, H.; Fehlhammer, W. P. Isocyanid- und Heteroallen-verbrückte Metallkomplexe, IX. Di- und Trieisenkomplexe mit funktionellen Isocyanidbrücken. *Chem. Ber.* **1992**, 125, 1093–1100.

(57) Goresky, S. I.; Ghosh, S.; Solomon, E. I. Mechanism of N_2O Reduction by the $\mu^4\text{-S}$ Tetranuclear Cu Z Cluster of Nitrous Oxide Reductase. *J. Am. Chem. Soc.* **2006**, 128, 278–290.

(58) Mazzoni, R.; Gabiccini, A.; Cesari, C.; Zanotti, V.; Gualandi, I.; Tonelli, D. Diiron complexes bearing bridging hydrocarbyl ligands as electrocatalysts for proton reduction. *Organometallics* **2015**, 34, 3228–3235.

(59) Krejčík, M.; Daněk, M.; Hartl, F. Simple construction of an infrared optically transparent thin-layer electrochemical cell: Applications to the redox reactions of ferrocene, $\text{Mn}_2(\text{CO})_{10}$ and $\text{Mn}(\text{CO})_3(3,5\text{-di-}t\text{-butyl-catecholate})$. *J. Electroanal. Chem.* **1991**, 317, 179–187.

(60) Fabrizi de Biani, F.; Ienco, A.; Laschi, F.; Leoni, P.; Marchetti, F.; Marchetti, L.; Mealli, C.; Zanello, P. Formation and Characterization of the Hexanuclear Platinum Cluster $[\text{Pt}_6(\mu\text{-PBUt}^t)_4(\text{CO})_6] \cdot (\text{CF}_3\text{SO}_3)_2$ through Structural, Electrochemical, and Computational Analyses. *J. Am. Chem. Soc.* **2005**, 127, 3076–3089.

(61) Arrigoni, F.; Bertini, L.; De Gioia, L.; Cingolani, A.; Mazzoni, R.; Zanotti, V.; Zampella, G. Mechanistic Insight into Electrocatalytic H_2 Production by $[\text{Fe}_2(\text{CN})\{\mu\text{-CN}(\text{Me})_2\}(\mu\text{-CO})(\text{CO})(\text{Cp})_2]$: Effects of Dithiolate Replacement in $[\text{FeFe}]$ Hydrogenase Models. *Inorg. Chem.* **2017**, 56, 13852–13864.

(62) Hillard, E. A.; de Abreu, F. C.; Ferreira, D. C. M.; Jaouen, G.; Goulart, M. O. F.; Amatore, C. Electrochemical parameters and techniques in drug development, with an emphasis on quinones and related compounds. *Chem. Commun.* **2008**, 2612–2628.

(63) Reisner, E.; Arion, V. B.; Guedes da Silva, M. F. C.; Lichtenecker, R.; Eichinger, A.; Keppler, B. K.; Kukushkin, V. Y.; Pombeiro, A. J. L. Tuning of Redox Potentials for the Design of Ruthenium Anticancer Drugs - an Electrochemical Study of $[\text{trans-RuCl}_4(\text{DMSO})]^-$ and $[\text{trans-RuCl}_4\text{L}_2]^-$ Complexes, where $\text{L} = \text{Imidazole}$, $1,2,4\text{-Triazole}$, Indazole . *Inorg. Chem.* **2004**, 43, 7083–7093.

- (64) Kirilin, W. G.; Cai, J.; Thompson, S. A.; Diaz, D.; Kavanagh, T. J.; Jones, D. P. Glutathione Redox Potential in Response to Differentiation and Enzyme Inducers. *Free Radical Biol. Med.* **1999**, *27*, 1208–1218.
- (65) In both cases, water/CD₃OD mixtures (5:2 v/v) were used to achieve a concentration of the diiron compound which is appropriate for ¹H NMR.
- (66) Compound [3]CF₃SO₃ resulted significantly less active than [2]CF₃SO₃ in terms of IC₅₀ data ROS production (vide infra). Therefore, it is reasonable to neglect the influence of the [Fe₂Cp₂(CO)(CNPh)(μ-CO){μ-CN(Me)(Ph)}]⁺ byproduct on the biological data of [3]CF₃SO₃.
- (67) Kunz-Schughart, L. A.; Freyer, J. P.; Hofstaedter, F.; Ebner, R. T. J. The use of 3-D cultures for high-throughput screening: the multicellular spheroid model. *J. Biomol. Screen.* **2004**, *9*, 273–285.
- (68) Menges, F. "Spectragryph-Optical Spectroscopy Software", Version 1.2.16.1, 2016–2022. <http://www.ffmpeg2.de/spectragryph>.
- (69) Fulmer, G. R.; Miller, A. J. M.; Sherden, N. H.; Gottlieb, H. E.; Nudelman, A.; Stoltz, B. M.; Bercau, J. E.; Goldberg, K. I. NMR Chemical Shifts of Trace Impurities: Common Laboratory Solvents, Organics, and Gases in Deuterated Solvents Relevant to the Organometallic Chemist. *Organometallics* **2010**, *29*, 2176–2179.
- (70) Willker, W.; Leibfritz, D.; Kerssebaum, R.; Bermel, W. Gradient selection in inverse heteronuclear correlation spectroscopy. *Magn. Reson. Chem.* **1993**, *31*, 287–292.
- (71) Holovics, T. C.; Deplazes, S. F.; Toriyama, M.; Powell, D. R.; Lushington, G. H.; Barybin, M. V. Organometallic Isocyanocyclopentadienides: A Combined Synthetic, Spectroscopic, Structural, Electrochemical and Theoretical Investigation. *Organometallics* **2004**, *23*, 2927–2938.
- (72) Sethi, S.; Das, P. K.; Behera, N. The chemistry of aminoferrocene, Fe{(η⁵-C₅H₄NH₂)(Cp)}: Synthesis, reactivity and applications. *J. Organomet. Chem.* **2016**, *824*, 140–165.
- (73) Weber, W. P.; Gokel, G. W.; Ugi, I. K. Phase Transfer Catalysis in the Hofmann Carbylamine Reaction. *Angew. Chem., Int. Ed.* **1972**, *11*, 530–531.
- (74) Kim, B.; Beebe, J. M.; Jun, Y.; Zhu, X.-Y.; Frisbie, C. D. Correlation between HOMO Alignment and Contact Resistance in Molecular Junctions: Aromatic Thiols versus Aromatic Isocyanides. *J. Am. Chem. Soc.* **2006**, *128*, 4970–4971.
- (75) Zakrzewski, J.; Krawczyk, M. Synthesis and Pesticidal Properties of Thio and Seleno Analogs of Some Common Urea Herbicides. *Phosphorus, Sulfur, Silicon Relat. Elem.* **2009**, *184*, 1880–1903.
- (76) Dhake, K. P.; Tambade, P. J.; Singhal, R. S.; Bhanage, B. M. An efficient, catalyst- and solvent-free N-formylation of aromatic and aliphatic amines. *Green Chem. Lett. Rev.* **2011**, *4*, 151–157.
- (77) Lacerda, R. B.; de Lima, C. K. F.; da Silva, L. L.; Romeiro, N. C.; Miranda, A. L. P.; Barreiro, E. J.; Fraga, C. A. M. Discovery of novel analgesic and anti-inflammatory 3-arylamine-imidazo[1,2-a]-pyridine symbiotic prototypes. *Bioorg. Med. Chem.* **2009**, *17*, 74–84.
- (78) Leifert, D.; Artiukhin, D. G.; Neugebauer, J.; Galstyan, A.; Strassert, C. A.; Studer, A. Radical perfluoroalkylation - easy access to 2-perfluoroalkylindol-3-imines via electron catalysis. *Chem. Commun.* **2016**, *52*, 5997–6000.
- (79) Skoch, K.; Cisarova, I.; Stepnicka, P. Selective Gold-Catalysed Synthesis of Cyanamides and 1-Substituted 1H-Tetrazol-5-Amines from Isocyanides. *Chem.—Eur. J.* **2018**, *24*, 13788–13791.
- (80) Howell, J. A. S.; Matheson, T. W.; Mays, M. J. Carbon-13 Nuclear Magnetic Resonance Studies of Isonitrile Derivatives of Tetracarbonylbis-(η-cyclopentadienyl)di-iron. *J. Chem. Soc. Chem. Commun.* **1975**, 865–866.
- (81) Gross, M.; Jordan, J. Voltammetry At Glassy Carbon Electrodes. *Pure Appl. Chem.* **1984**, *56*, 1095–1129.
- (82) Grimme, S.; Brandenburg, J. G.; Bannwarth, C.; Hansen, A. A. Consistent structures and interactions by density functional theory with small atomic orbital basis sets. *J. Chem. Phys.* **2015**, *143*, 054107.
- (83) Weigend, F.; Ahlrichs, R. Balanced basis sets of split valence, triple zeta valence and quadruple zeta valence quality for H to Rn: Design and assessment of accuracy. *Phys. Chem. Chem. Phys.* **2005**, *7*, 3297–3305.
- (84) Weigend, F. Accurate Coulomb-fitting basis sets for H to Rn. *Phys. Chem. Chem. Phys.* **2006**, *8*, 1057–1065.
- (85) Kruse, H.; Grimme, S. A geometrical correction for the inter- and intra-molecular basis set superposition error in Hartree-Fock and density functional theory calculations for large systems. *J. Chem. Phys.* **2012**, *136*, 154101.
- (86) Grimme, S.; Ehrlich, S.; Goerigk, L. Effect of the damping function in dispersion corrected density functional theory. *J. Comput. Chem.* **2011**, *32*, 1456–1465.
- (87) Grimme, S.; Antony, J.; Ehrlich, S.; Krieg, H. A consistent and accurate ab initio parametrization of density functional dispersion correction (DFT-D) for the 94 elements H-Pu. *J. Chem. Phys.* **2010**, *132*, 154104.
- (88) Cossi, M.; Rega, N.; Scalmani, G.; Barone, V. Energies, structures, and electronic properties of molecules in solution with the C-PCM solvation model. *J. Comput. Chem.* **2003**, *24*, 669–681.
- (89) Barone, V.; Cossi, M. Quantum Calculation of Molecular Energies and Energy Gradients in Solution by a Conductor Solvent Model. *J. Phys. Chem. A* **1998**, *102*, 1995–2001.
- (90) Cramer, C. J. *Essentials of Computational Chemistry*, 2nd ed.; Wiley: Chichester, 2004.
- (91) Neese, F. Software update: The ORCA program system - Version 5.0. *Wiley Interdiscip. Rev. Comput. Mol. Sci.* **2022**, *12*, No. e1616.
- (92) Lu, T.; Chen, F. Multiwfn: A multifunctional wavefunction analyzer. *J. Comput. Chem.* **2012**, *33*, 580–592.
- (93) Dearden, J. C.; Bresnen, G. M. The Measurement of Partition Coefficients. *Quant. Struct.-Act. Relat.* **1988**, *7*, 133–144.
- (94) Bresciani, G.; Busto, N. V.; Ceccherini, V.; Bortoluzzi, M.; Pampaloni, G.; Garcia, B.; Marchetti, F. Screening the biological properties of transition metal carbamates reveals gold(I) and silver(I) complexes as potent cytotoxic and antimicrobial agents. *J. Inorg. Biochem.* **2022**, *227*, 111667.
- (95) (a) Calculated by the formula pD = pH* + 0.4, where pH* is the value measured for H₂O-calibrated pH-meter Westcott, C. C. *pH Measurements*; Academic Press: New York, 1978. (b) Covington, A. K.; Paabo, M.; Robinson, R. A.; Bates, R. G. Use of the glass electrode in deuterium oxide and the relation between the standardized pD (paD) scale and the operational pH in heavy water. *Anal. Chem.* **1968**, *40*, 700–706.
- (96) Harper, B. W. J.; Petruzzella, E.; Sirota, R.; Faccioli, F. F.; Aldrich-Wright, J. R.; Gandin, V.; Gibson, D. Synthesis, characterization and in vitro and in vivo anticancer activity of Pt(IV) derivatives of [Pt(1S,2S-DACH)(5,6-dimethyl-1,10-phenanthroline)]. *Dalton Trans.* **2017**, *46*, 7005–7019.
- (97) Gandin, V.; Ceresa, C.; Esposito, G.; Indraccolo, S.; Porchia, M.; Tisato, F.; Santini, C.; Pellei, M.; Marzano, C. Therapeutic potential of the phosphino Cu(I) complex (HydroCuP) in the treatment of solid tumors. *Sci. Rep.* **2017**, *7*, 13936.